Understanding instability in hybrid stepper motors

Stolte, J.

Award date:
2006

Eindhoven University of Technology
Department of Electrical Engineering
Control Systems

TU/e technische universiteit eindhoven

Understanding instability in hybrid stepper motors

by

J. Stolte

Master of Science thesis

Project period: april 2006
Report Number: 06A/05
Supervisors:
prof.dr.ir. P.P.J. van den Bosch
Dr. ir. A. Veltman (TU/e)

Additional Commission members:
Prof.dr.ir. A.J.A. Vandenput (TU/e)
Ir. J. van Gerwen (Bosch-Rexroth)
Ir. L. Idema (Océ)

Understanding instability in hybrid stepper motors

Master thesis by Jasper Stolte

Abstract— **Research into hybrid stepper motors peaked in the late 1970's, and as such there is very little recent literature on the fundamental workings of them. Especially the problem of parametric instability when driven in open loop is a poorly understood phenomenon. Most users just accept it as a given and stay away from the region of instability. Literature accurately describing the instability in hybrid stepper motors is very hard to find.**

This paper demonstrates the effect that causes the instability, and predicts exactly for what frequency range to expect the open loop instability. Viscous damping has a very profound stabilising effect on the stepper motor. A stability criterion is formulated both for motors without any damping and for motors that do have damping.

Also, a control strategy is proposed based on adjusting the amplitude of the voltage source such that it removes energy from oscillations superimposed on the steady state rotation. The controller uses an observer to estimate the rotor load angle from the motor back-emf signals.

List of symbols

R	=	stator resistance	[Ω]
L	=	phase inductance	[H]
T	=	torque produced	[Nm]
T_l	=	load torque	[Nm]
B	=	mechanical friction	[$\frac{Nms}{rad}$]
θ	=	absolute rotor angle	[rad]
ω	=	absolute rotor angular speed	[$\frac{rad}{s}$]
V	=	amplitude of applied voltage	[ ]
$v_{\alpha,\beta}$	=	instantaneous phase voltages	[V]
$i_{\alpha,\beta}$	=	instantaneous phase currents	[A]
$v_{d,q}$	=	instantaneous voltage in (d,q)	[V]
$i_{d,q}$	=	instantaneous current in (d,q)	[A]
p	=	number of rotor poles	[ ]
λ_m	=	flux linkage due to the magnet	[$\frac{Vs}{rad}$]

I. Introduction

1.1. Background

Hybrid stepper motors are an interesting type of electrical machine. They are synchronous motors, because the built-in magnet rotates at the same speed as the input signals. With the most common drive types, the stepper motor does not rotate smoothly but rather moves a fixed amount every time the drive changes the applied voltages. This stepping movement of stepper motors allows these motors to run without an incremental encoder or resolver for shaft angle measurement. Together with other advantages such as good durability, low price, and non cumulative positional error this makes the stepper motor suitable for application in scanners, printers and other computer peripherals.

One of the biggest disadvantages of driving stepper motors without an incremental encoder is that stepper motors are famous for their inherent instability. Apart from the usual mechanical resonance commonly found in electrical machines at low frequencies they also suffer from stability problems at much higher frequencies. This instability is inherent to the stepper motor and can cause the motor to stall especially when they are driven in open loop. The precise nature of the instability was more closely investigated in the 1970's [1], [2], [4], [6].

Stepper motors cannot be driven in the instability region when they are voltage driven in open loop. A possible solution to overcome this is to use a current driver, but care must be taken to have sufficient voltage available to make a good current driver. The rotating magnet in stepper motors produces a voltage in the stator windings which is called back-emf, or just emf for short. Because this voltage opposes the driver voltage, the remaining voltage to make current drops with rotation speeds. To force current driving at the frequency range of instability the available voltage would need to be impractically high.

Several strategies have been developed to counter the instability, which can be roughly divided into three main groups:

- Adding damping through friction, controllable brakes, inertial damping, rubber suspension or other mechanical means. These solutions add some mechanical part to the stepper motor which takes away energy from growing oscillations by heating up.
- Adding and/or maximizing electronic damping by choosing an appropriate driving scheme. For instance, two-phase on has better damping than one phase on [4]. But also elaborate electronic circuits have been designed to increase electronic damping [21].
- Introducing some form of feedback into the system, and using this feedback to control the stepper motor. Many schemes have been developed using encoders for positional feedback, see for instance [17], [18]. Another option is to use the back-emf voltages produced by the motor to close the loop [10], [15], [13]. Due to the ever increasing availability of faster and cheaper microcontrollers these options are gaining popularity.

This paper proposes a controller which falls into the third category. Due to the availability of cheap and fast processors and extra options such as driving with sine shaped voltages and currents almost all novel controller concepts utilize the back-emf to close the loop. Nevertheless, in most applications stepper motors are driven with full-step or half-step current drivers. This is inspired by the experience with other electric machines where motor torque is directly proportional to phase current. In stepper motors this is not always the case.

Viewing the stepper motor from the rotor gives a good understanding of the instability. The instability appears to be similar to the instability occurring in turbo-generators.

This work was conducted at Eindhoven University of Technology under the supervision of dr. ir. A. Veltman and prof. dr. ir. P.P.J. van den Bosch.

In turbo-generators the instability is controlled by adding a physical damping cage which suppresses oscillations superimposed on the synchronous frequency. The damping cage only produces torque when there is a difference in rotation speed between itself and the applied field. This paper proposes a control method that aims to add a simulated damping cage by interacting with the applied field and the phase currents the same way a physical damping cage in the motor would have. To achieve this the phase currents are measured and used to control the applied phase voltages.

1.2. Contributions

Although other publications have observed the phenomenon of instability, there is no easily understandable physical explanation for it. This paper not only shows when to expect instability, but also gives an intuitive explanation as to what causes it. Based on this understanding a control strategy is being proposed to counter the effects of instability.

1.3. Outline

The paper will start with a general stability analysis in section (2). An intuitive approach to the instability in stepper motors is given, and stability criteria are formulated. In the last section a controller and observer are demonstrated that stabilise the motor by adjusting the amplitude of the input voltage.

2. Stability Analysis

2.1. Basic model

Most hybrid stepper motors have two phases, which are mounted orthogonally to eachother, with respect to the magnetic field in the motor. When there are more than two phases it is possible to rewrite the model as a two phase model so in this paper only the two-phase model is considered. Each of the phases consists of a set of coils wound around salient iron structures. These coils have linked flux with the rotor magnet, and this magnetic coupling enables the motor to produce torque. The coils are modeled by an inductance L with a series resistance R modelling the winding resistance as well as possible added forcing resistance. The phase model is completed with an added voltage source representing the emf induced by the rotation of the magnet on the rotor. The model described is shown in figure 1.

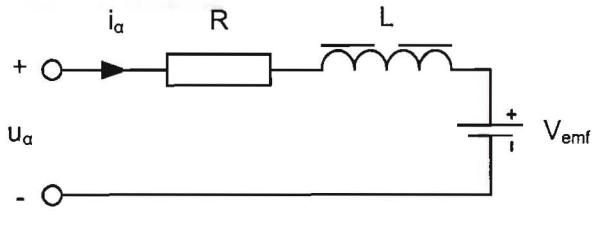

Fig. 1. Electrical equivalent model of one phase of the stepper motor.

The equations governing the electrical phase equivalents can easily be deduced. Next to the 'electrical' equations there is also a basic equation for the torque that is produced by the stepper motor, which consists of the phase currents compared to the direction of the magnet flux represented by $p\theta$. All three equations are stated together in (1).

$$v_\alpha = Ri_\alpha + L\frac{di_\alpha}{dt} + \frac{d}{dt}\left(\lambda_m cos(p\theta)\right) \quad (1a)$$

$$v_\beta = Ri_\beta + L\frac{di_\beta}{dt} + \frac{d}{dt}\left(\lambda_m sin(p\theta)\right) \quad (1b)$$

$$T = -p\lambda_m\left(i_\alpha sin(p\theta) - i_\beta cos(p\theta)\right) \quad (1c)$$

Note that this model does not include advanced effects such as magnetic saturation or hysteresis. For small hybrid stepper motors driven within specifications these effects do not play a significant role. The detent torque is neglected here as well as it is negligible compared to the torque produced by the phase currents.

A different effect that does have a significant impact on stepper motor dynamics is the frequency depence of the phase impedance. The skin effect is quite noticable in stepper motors. Due to the skin effect at higher frequencies the field lines will concentrate themselves in the outer layer of the material. That means less material is actually available, such that the impedance changes. The real part of the phase impedance which is modeled by resistance R increases significantly with frequency while the imaginary pary modeled by the motor inductance L decreases significantly with frequency. The skin effect can be included in models by actually making R and L dependent of the applied frequency or by introducing ladder networks. Including skin effect will make any model more accurate. However, since doing so only complicates things and does not improve understanding of the instability phenomenon the effect is left out here.

The per phase model of figure 1 is also applicable for permanent magnet stepper motors and variable reluctance stepper motors. Because the principle of operation for variable reluctance motors is different their equations for torque are different, and they are not considered in this paper.

2.2. State space model

To have a good basis for mathematical analysis of the system a state space model is built from (1). The phase currents are chosen as states for the electrical part of the system, and for the mechanical part the rotor angular speed and rotor angle are used. Rewriting (1) into state space format yields (2).

The standard model views the motor in (α, β) coordinates as then the currents correspond to the two actual phase currents of the two phase hybrid stepper motor. For further analysis it can be advantageous to view the motor from a different system of coordinates, the (d, q) coordinate system, that rotates synchronously with the rotor. In the (d, q) coordinate system the rotor and thus the permanent magnet flux will have a fixed orientation. Due to the transformatian the magnet flux always points in the same direction as the d-axis which will lead to an easier analysis of the dynamics. The coordinate transform is shown graphically in figure 2.

The (d, q) coordinate system makes one rotation for every cycle of the electrical signals in the motor. This is closely related to the number of rotor teeth p, since the electrical

$$\frac{d}{dt}\begin{pmatrix} i_\alpha \\ i_\beta \\ \omega \\ \theta \end{pmatrix} = \begin{pmatrix} -R/L & 0 & -p\lambda_m sin(p\theta)/L & 0 \\ 0 & -R/L & p\lambda_m cos(p\theta)/L & 0 \\ -p\lambda_m sin(p\theta)/J & p\lambda_m cos(p\theta)/J & -B/J & 0 \\ 0 & 0 & 1 & 0 \end{pmatrix} \begin{pmatrix} i_\alpha \\ i_\beta \\ \omega \\ \theta \end{pmatrix} + \begin{pmatrix} u_\alpha/L \\ u_\beta/L \\ -T_l/J \\ 0 \end{pmatrix} \tag{2}$$

$$\frac{d}{dt}\begin{pmatrix} i_d \\ i_q \\ \omega \\ \theta \end{pmatrix} = \begin{pmatrix} -R/L & p\omega & 0 & 0 \\ -p\omega & -R/L & -p\lambda_m/L & 0 \\ 0 & p\lambda_m/J & -B/J & 0 \\ 0 & 0 & 1 & 0 \end{pmatrix} \begin{pmatrix} i_d \\ i_q \\ \omega \\ \theta \end{pmatrix} + \begin{pmatrix} cos(p\theta) & sin(p\theta) & 0 \\ -sin(p\theta) & cos(p\theta) & 0 \\ 0 & 0 & 1 \\ 0 & 0 & 0 \end{pmatrix} \begin{pmatrix} u_\alpha/L \\ u_\beta/L \\ -T_l/J \end{pmatrix} \tag{3}$$

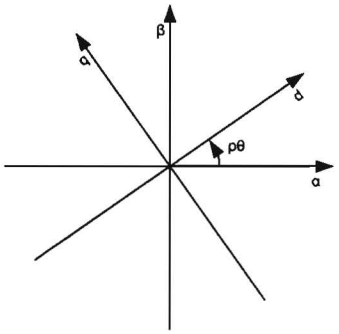

Fig. 2. Graphical representation of the transformation from (α, β) coordinates to (d, q) coordinates. The (d, q) coordinate system rotates p (the number of rotor teeth) times per period of θ, so it rotates once per full period of the electrical signals in steady state operation.

signals make one full cycle to move the rotor by one tooth. Therefore the (d, q) system makes p rotations per period of rotor angle θ. The equations realising the transformation of figure 2 are given in (4).

$$\begin{pmatrix} i_d \\ i_q \\ \omega \\ \theta \end{pmatrix} = \begin{pmatrix} cos(p\theta) & sin(p\theta) & 0 & 0 \\ -sin(p\theta) & cos(p\theta) & 0 & 0 \\ 0 & 0 & 1 & 0 \\ 0 & 0 & 0 & 1 \end{pmatrix} \begin{pmatrix} i_\alpha \\ i_\beta \\ \omega \\ \theta \end{pmatrix} \tag{4}$$

The result of applying the coordinate transform (4) on the stepper motor model (2) is a new state space model in which the orientation between the currents i_d and i_q and the rotor magnet flux direction is fixed. The resulting model is given as (3).

In (3) the phase voltages have not yet been filled in, and are still in (α, β) coordinates. For this analysis it is assumed the applied voltage is of sinusoidal shape, which greatly simplifies the analysis. This is not a big constraint since for true steady state operation the phase currents need to be sinusoidal, for which a sinusoidal shaped voltage is needed as well. For steady state rotation the applied frequency should be p times the angular frequency of the rotor. In that case the applied voltage vector becomes a constant vector in the (d, q) coordinate system. A load angle δ is included to obtain the required torque. The resulting steady state voltages are described by (5).

$$\begin{aligned} u_\alpha &= V cos(p\omega t + \delta) = V cos(p\theta + \delta) \\ u_\beta &= V sin(p\omega t + \delta) = V sin(p\theta + \delta) \end{aligned} \tag{5}$$

The graphical representation of the applied voltages is shown in figure 3. Note that the permanent magnet flux Φ_m is always pointing in the direction of the d-axis due to the transformation of coordinates from (α, β) to (d, q). The angle δ indicates the angle the applied voltage vector is ahead of the d-axis, and therefore the angle between the applied voltage and the permanent magnet flux.

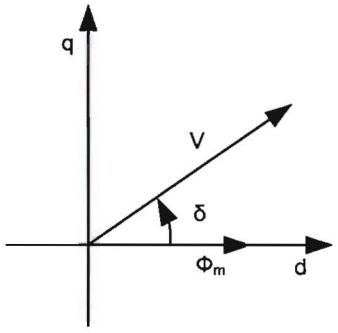

Fig. 3. The angle δ is defined as the angle the applied voltage vector is ahead of the permanent magnet flux, which is always parallel to the d-axis.

2.3. Finding the operating point

If the voltages given in (5) are applied to the system of (3) the resulting system is given by (6). The steady state values for i_d, i_q and δ can be derived from (6) by setting $\frac{di_d}{dt} = \frac{di_q}{dt} = \frac{d\omega}{dt} = 0$. In steady state the load angle δ will become a constant yielding a surprisingly simple and elegant system of equations. Of course, a meaningful solution can only be found when the stepper motor can produce enough torque to overcome both the friction and the load torque. When this is the case steady state operation is described by (7).

$$i_q = \frac{B\omega + T_l}{p\lambda_m} \tag{7a}$$

$$X = \frac{p\lambda_m R\omega}{V\sqrt{R^2 + p^2\omega^2 L^2}} + \frac{(B\omega + T_l)\sqrt{R^2 + \omega^2 L^2}}{p\lambda_m V}$$

$$\delta = \arcsin(X) + \arctan\left(\frac{p\omega L}{R}\right) \tag{7b}$$

$$i_d = \frac{p\omega L}{R} i_q + \frac{V}{R}\cos(\delta) \tag{7c}$$

The calculations of these operating points are shown in appendix I. The formulas for the operating points are rather

$$\frac{d}{dt}\begin{pmatrix} i_d \\ i_q \\ \omega \\ \theta \end{pmatrix} = \begin{pmatrix} -R/L & p\omega & 0 & 0 \\ -p\omega & -R/L & -p\lambda_m/L & 0 \\ 0 & p\lambda_m/J & -B/J & 0 \\ 0 & 0 & 1 & 0 \end{pmatrix}\begin{pmatrix} i_d \\ i_q \\ \omega \\ \theta \end{pmatrix} + \begin{pmatrix} V cos(\delta)/L \\ V sin(\delta)/L \\ -T_l/J \\ 0 \end{pmatrix} \tag{6}$$

cumbersome, and do not give insight into the dynamics directly. To gain better understanding it is useful to start analysis with a more simple version, setting the mechanical friction parameter B and the load torque T_l to zero. In this case the stepper motor does not have to deliver any torque in steady state, and therefore i_q will be zero as well. When B and T_l are set to zero, (7) reduces to (8).

$$\delta = \arcsin\left(\frac{p\lambda_m R\omega}{V\sqrt{R^2 + p^2\omega^2 L^2}}\right) + \arctan\left(\frac{p\omega L}{R}\right) \tag{8a}$$

$$i_d = \frac{V}{R}\cos\delta \tag{8b}$$

$$i_q = 0 \tag{8c}$$

As a function of frequency, the load angle δ starts at zero, and asymptotically increases to its limit value of $\arcsin(\frac{R\lambda_m}{VL}) + \frac{\pi}{2}$. Note that when $B = 0$ and $0 < \frac{R\lambda_m}{VL} < 1$ the argument of the *arcsine* will always be smaller than 1 meaning that there is always a valid (but not necessarily stable) operating point for δ. When $\frac{R\lambda_m}{VL}$ becomes larger than 1, there will be a frequency at which the argument for the *arcsine* becomes larger than 1 as well, showing that no meaningful steady state solution is possible. Physically this means the emf generated by the magnet will become too large compared to the applied voltage.

Also note that the maximum feasible value (also for $B > 0$) for the load angle δ is π, as both the *arcsine* function and the arctangent function have $\frac{\pi}{2}$ as maximum output. This agrees with general motor theory which dictates maximum power is produced when the voltage vector is 180 degrees ahead of the magnet. In practice this point is metastable such that due to noise the motor cannot be driven at the maximum power point in steady state. A practical example of a steady state voltage vector for a stepper with a load torque is shown in figure 4.

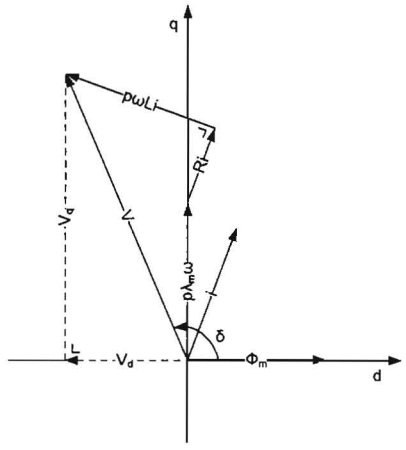

Fig. 4. Voltage in the motor based on various components. The total voltage vector is the sum of V_q and V_d. Note that $i_q > 0$ in this case which means that the motor produces torque, so there is either a load torque or some friction.

R	=	5.5	Ω
L	=	$7.4 \cdot 10^{-3}$	H
V	=	12	V
B	=	0	N-m-s-rad^{-1}
p	=	50	
J	=	$2.8 \cdot 10^{-6}$	kg-m^2
λ_m	=	$1.4 \cdot 10^{-3}$	V-s-rad^{-1}

TABLE I

PARAMETERS FOR THE MINEBEA 17PM-K223 WHEN IT IS VOLTAGE DRIVEN AT 12V. NOTE THAT AT LOW FREQUENCIES THIS MEANS THE CURRENT WILL BE FAR MORE THAN THE RATED CURRENT OF 0.6 A.

2.4. Local stability

Once an operating point has been established the local stability of this point can be analysed using a linearised version of the stepper motor model. The linearised version of (6) is given in (9). The local stability can be determined by inspection of the eigenvalues of (9). In this paper, the stability for the 17PM-K223 motor by Minebea is examined more closely. The motor parameters for this motor are listed in table I.

Note that when stepper motors are voltage driven it is appropriate to scale the voltage with frequency (Volts per Hertz drive), so the current is approximately the same for all frequencies. Because this only makes the stability analysis less transparant and does not make a fundamental difference for the analysis a constant voltage amplitude is used here. The poles resulting from these parameters as a function of frequency are shown in 5.

Obviously, there are four poles for the system as there are four states. The root locus as shown in figure 5 is typical for stepper motor behaviour as it shows two poles in the far left halfplane, and two poles more close to the origin. The two poles in the far left are associated with the electrical circuit, and are influenced only little by the mechanical part of the system. The two poles closer to the origin are associated with the mechanical part of the system and their trajectories are greatly influenced by both the electrical parameters and the mechanical parameters. These poles are the ones that cause instability since their real parts can become positive which results in an instable operating point. The trajectories of these poles are magnified in figure 6.

From this plot it can be seen that the motor is stable for low frequencies, but when the stator excitation frequency becomes higher at some point the poles from the linearised system will travel into the right half plane making the motor behaviour unstable. From literature it becomes clear that the frequency

$$\frac{d}{dt}\begin{pmatrix}\delta i_d\\ \delta i_q\\ \delta\omega\\ \delta\theta\end{pmatrix}=\begin{pmatrix}-R/L & p\omega & pi_q & pVsin(\delta)/L\\ -p\omega & -R/L & -(pi_d+p\lambda_m/L) & -pVcos(\delta)/L\\ 0 & p\lambda_m/J & -B/J & 0\\ 0 & 0 & 1 & 0\end{pmatrix}\begin{pmatrix}\delta i_d\\ \delta i_q\\ \delta\omega\\ \delta\theta\end{pmatrix} \tag{9}$$

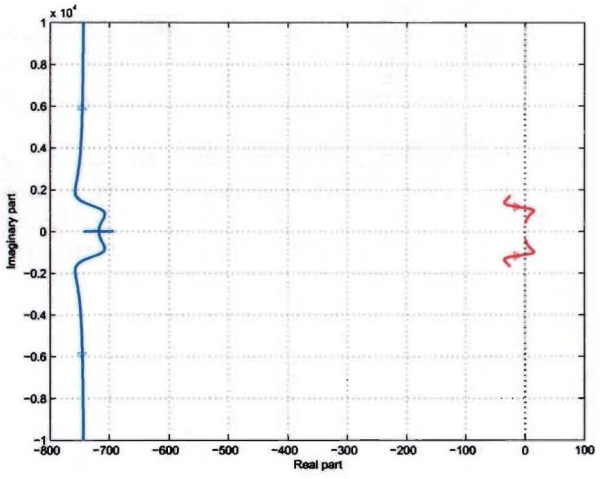

Fig. 5. Root locus in the s-plane of the linearised system (9) as a function of frequency ω.

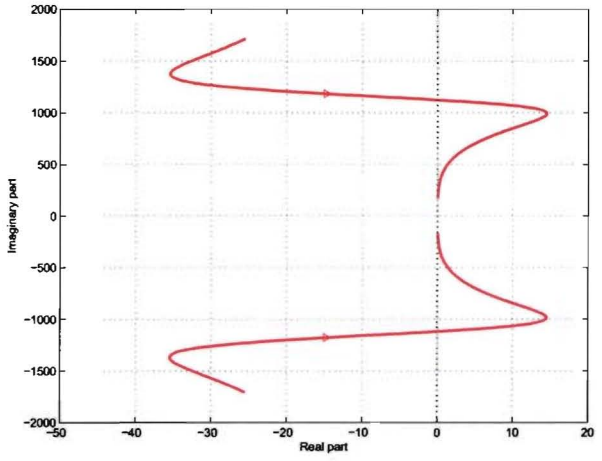

Fig. 6. Zoomed in view of figure 5 on the poles close to the origin. Note that the real part of these poles starts in the left half plane, and at some frequency cross the boundary into the right half plane. For very high frequency the poles will approach zero but stay in the right half plane.

for which this happens is closely linked to the ratio between the phase resistance R and the phase inductance L [1], [5]. The instability will occur when $p\omega > \frac{R}{L}$. The precise reason for this was so far not given in literature, but this will be explained in subsection 7.

Note that the instability occurs even in this simple model with a sinusoidal voltage drive. That means the instability is not caused by the stepped way of driving the stepper motor but rather it is a feature inherent to the stepper motor itself.

2.5. *Introducing damping to the system*

When the damping B is not equal to zero, which is physically reasonable, the full equations of (7) have to be taken into account. Introducing damping means torque has to be delivered by the motor for steady state rotation. Therefore the i_q needs to be greater, and to realise that the load angle δ will be greater as well. Because the load angle increases i_d will be smaller.

Due to the damping term for increasing frequency the argument of the *arcsine* function in (7a) will eventually become greater than one such that there will be no feasible value for δ. Physically this means the motor cannot produce the torque needed to overcome the damping torque and will stall (pull-out frequency). The root locus for the system with a damping parameter of $B = 5 \cdot 10{-}5$ N-m-s-rad^{-1} is shown in figure 7.

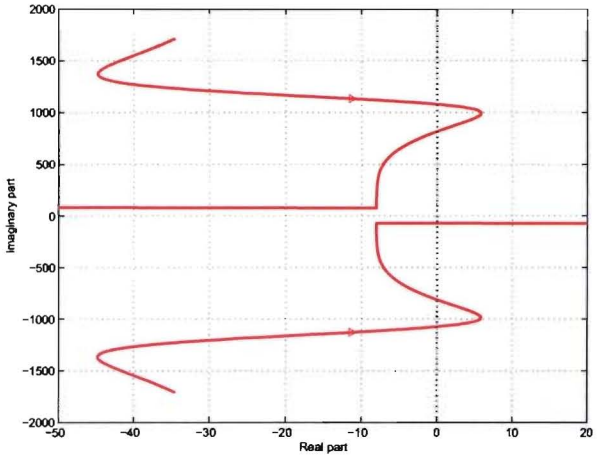

Fig. 7. Locus of K223 motor as a function of frequency with a damping parameter B of $5{\cdot}10{-}5$ N-m-s-rad^{-1}. The locus shows the same behaviour as the locus without damping from figure 6 but it is shifted somewhat to the left.

The root locus for the system with damping resembles the root locus from the system without damping from figure 6 closely. The main difference lies in a shift of the locus as a whole to the left. The horizontal breakaway at high frequency is caused by the system not having a feasible steady state solution. Because the locus is shifted to the left there is now another stable region for higher frequencies, which concurs with findings in literature [1], [2]. When the damping parameter is increased even further the whole locus will be in the left half plane so the motor is stable over the whole frequency range.

So the instability problem could be solved by adding extra damping to the system, which is a very simple thing to do. The price that is payed for adding extra damping is that the damper

will be dissipating energy also at frequencies where there was no instability. This energy is lost, which makes adding dampers inefficient. Apart from that the braking torque caused by the $B\omega$ becomes large for high frequencies, meaning that the motor will stall for much lower frequencies than it would without this damping. Another form of damping is inertial damping, which does not limit the maximum operating frequency. Inertial dampers do however restrict the dynamic performance and introduce additional physical constraints on the system due to their size.

2.6. *Almost no stability dependence on inertia*

It is very interesting to note that the stepper motor qualitative behaviour depends only very little of the rotating inertia. The exact relation between inertia and stability is demonstrated in section 7 and appendix II, but for now can be neglected. This means that the frequency at which the instability occurs does not depend on the inertia attached to the rotor. Of course, the inertia does have an effect on the quantitative behaviour of the system with more inertia leading to a slower system as a whole. This is reflected in the root locus as well, which does not change in shape for different inertias. What actually happens is that for larger inertias the whole root locus is compressed towards zero. This means the poles will always be closer to the imaginary axis which results in lower eigenfrequencies. Since the absolute damping remains the same, the relative damping decreases when the inertia increases. Therefore it will take longer for transients to die away, even though the motor is still stable. The root locus for two different inertias is shown in figure 8.

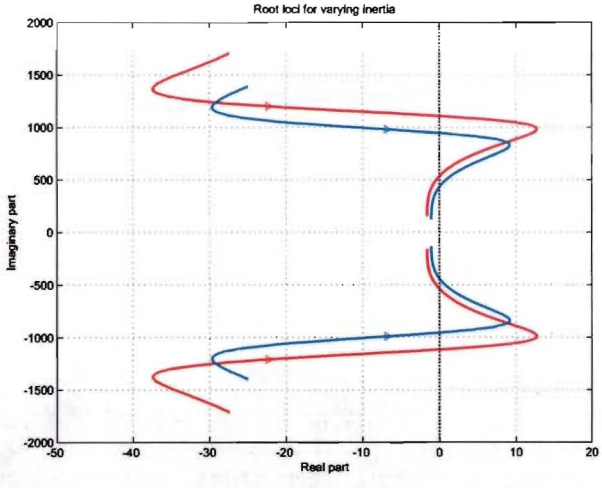

Fig. 8. Locus change for two different inertias. The red locus is the same as in previous experiments, while the blue locus is associated with a 50% increase in inertia.

Note that although the stability of the motor does not depend on the inertia the system performance will be degraded for high rotating inertias. The maximum acceleration of the system will be limited by the ratio of available torque and inertia which will drop for higher inertias. And due to the longer transients the time to reach steady state rotation will increase.

2.7. *Making sense of instability*

This subsection aims to give a good intuitive understanding what causes the instability, and at what frequencies to expect it. From literature it is known that in many stepper motors the instability region starts at a frequency of $p\omega = \frac{R}{L}$. Sometimes however, the frequency at which instability starts is much higher. Why the instabilty normally starts at $p\omega = \frac{R}{L}$, and why it sometimes deviates is not explained by earlier work. Through more thorough analysis of the linearised system a relatively simple equation can be obtained showing when to expect instability.

It is important to understand what effect physically causes the instability in the first place. When the motor is rotating in steady state, and there is a small disturbance in the rotor angular speed ω the emf produced by the magnet will be slightly larger for positive deviation, and slightly smaller for negative deviation. This emf difference leads to a change in the total voltage over the phases, and through this to deviating phase currents. The torque produced by the motor is directly dependent of the current in the q-axis of the motor. Now if an initial increase in the rotor speed ω leads to a decreasing i_q the motor will produce less torque which will cause ω to decrease again, thus having a stabilising effect. However for higher frequencies an increase in the rotor speed will lead to an emf vector causing an increase of i_q which can cause the motor to become unstable.

To see when this happens we consider an intermediate result for i_q as calculated in appendix (I). The equation of interest is (21), which is restated here as (10).

$$i_q = \frac{V}{\sqrt{R^2 + p^2\omega^2 L^2}} \sin(\delta - \phi_o) - \frac{p\lambda_m \omega R}{R^2 + p^2\omega^2 L^2} \qquad (10)$$

The second part of (10) is the emf contribution to i_q, which is only dependent of system parameters and rotor speed ω. It is not dependent of the source voltage or load angle at which the motor operates. The contribution of the second part including its first and second derivate with respect to rotor speed ω are shown in figure 9.

The emf contribution to i_q is a curve similar to the torque curve of an induction machine. The contribution is symmetrical around $\omega = 0$, and has maximum values for $p\omega = \pm\frac{R}{L}$. The first derivative of the emf contribution with respect to ω is negative around $\omega = 0$ which means that rising rotor speed ω will lead to falling current in the q-axis and thus to lower torque being produced. This will cause the rotor speed to fall again, and therefore is a stabilising effect. However, when the frequency rises above the threshold of $p\omega = \pm\frac{R}{L}$ the change in i_q will produce a torque that amplifies the change in rotor speed, such that the effect is destabilising.

Whether or not the motor actually becomes instable above $p\omega = \pm\frac{R}{L}$ depends on the rest of the system. The linearised version of the system becomes unstable when at least one of the eigenvalues of the linearised system matrix has positive real value. It is possible to analyse the eigenvalues of the linearised matrix analytically, which results in an analytical expression for the instability boundary. The calculation of this

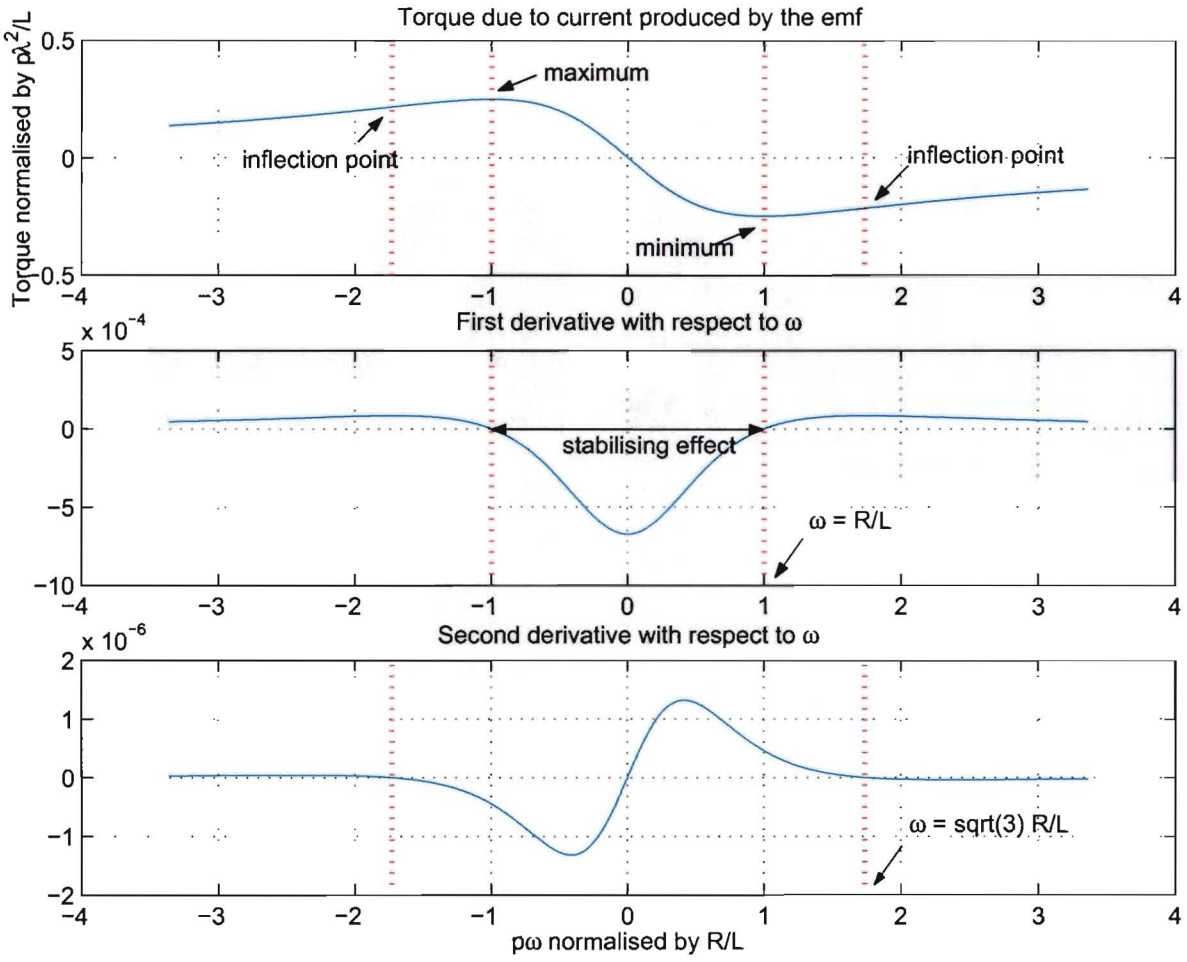

Fig. 9. Braking torque produced by current produced by emf voltage in steady state as a function of frequency ω. The torque resembles the torque curve of an induction motor. There is a minimum torque at frequency $p\omega = \sqrt{3}\frac{R}{L}$, which means for higher frequencies the derivative becomes positive. A positive derivative generates a destabilising effect because the change in produced torque due to small disturbances in ω amplify the disturbance rather than dampening it.

boundary is given in appendix II. When the damping is zero, instability is reached when:

$$(\sqrt{R^2 + p^2\omega^2 L^2} + \frac{p\lambda_m L p\lambda_m}{2J\sqrt{R^2+p^2\omega^2L^2}})(i_d + \frac{\lambda_m}{2L}) \\ -V\sin(\delta + \arctan(\frac{R}{p\omega L})) < 0 \qquad (11)$$

For frequency zero, the motor is stable as $\frac{\lambda_m}{2L} > 0$. For increasing frequency the expression as a whole decreases monotonously, and at a certain point the instability border is crossed. The frequency for which this happens will lie very close to $p\omega = \frac{R}{L}$ when the inertia J is large, and will be higher than that when the inertia is very small. The criterion for the Minebea K223 is shown in figure 10. The K223 is a very small motor with a small inertia such that instability is only reached at well over twice the expected frequency.

Neglecting the inertia dependent part, the instability can be intuitively understood. The instability occurs when the voltage in the d-axis $((pi_d + \frac{p\lambda_m}{2L})\sqrt{R^2 + p^2\omega^2L^2})$ is not enough to compensate the voltage in the d-axis demanded by the load $(V\sin(\delta + \arctan(\frac{R}{p\omega L}))$.

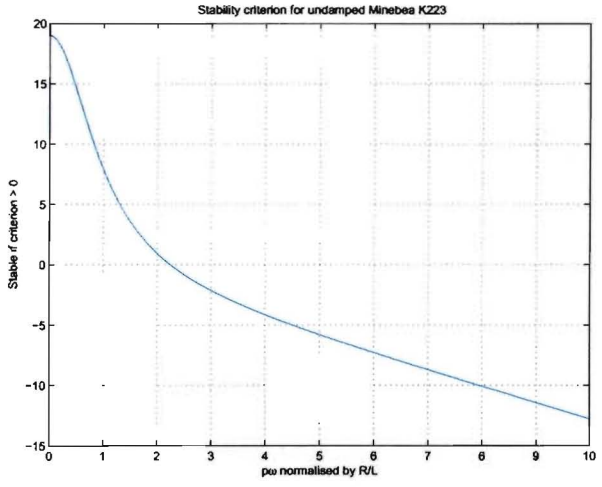

Fig. 10. The motor stability criterion against normalised frequency. The K223 is a small motor with a very small inertia, such that the instability occurs much later than excpected. For a motor without damping the criterion will always have negative slope in ω.

Introducing damping to the stepper motor makes it more stable, since the damping always dissipates energy from the disturbance oscillations. Appendix III shows the calculation of the stability boundary for the motor with damping. Including damping, and again neglecting the inertia terms the motor will be stable if:

$$\begin{aligned} &B(R^2+p^2\omega^2L^2)\left(2\tfrac{R}{L}((\tfrac{RJ+BL}{J})^2+p^2\omega^2L^2)\right)\\ &+Rp\lambda_m(2pi_dL+p\lambda_m)\left(2\tfrac{R}{L}((\tfrac{RJ+BL}{J})^2+p^2\omega^2L^2)\right)\\ &-\left(\tfrac{2RJ+BL}{J}\right)^2(p\lambda_m pV(R\cos(\delta)+p\omega L\sin(\delta)))>0 \end{aligned} \tag{12}$$

An extra stabilising term is introduced, which is scaled by $B(R^2+p^2\omega^2L^2)$. The contribution of this term rises with frequency, which can be explained physically because the friction torque produced by the damping rises with frequency. The damping term grows quadratically with the frequency, while the destabilising terms drops only linearly. Therefore for high enough frequencies the motor will reach a stable area again. Naturally this only holds if there is a valid operating point, meaning the motor can produce enough torque to overcome the damping friction. If enough damping is introduced the motor will be stable for all frequencies.

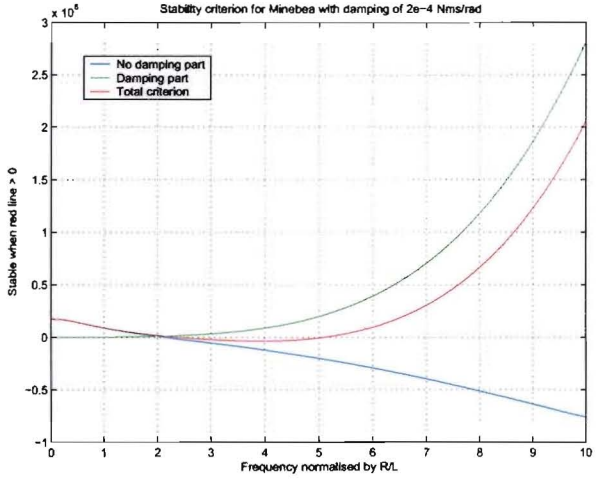

Fig. 11. The stability criterion for the hybrid stepper motor including damping. The blue line is almost the same as in the no-damping case. The green line is the extra time introduced by the damping, and the red line is the combination of the two. Because the red line grows quadratically while the blue falls only linearly the motor will always reach another stable area for higher frequencies.

Introducing damping also has a downside, since for very high frequencies the motor cannot produce enough torque to overcome the damping torque. That means that for those frequencies the motor cannot rotate in steady state. This effect is represented because for those frequencies there no valid operation point can be found for the system.

3. Proposed Control Method

In the previous section the instability was shown to be caused by current produced by the emf. For certain frequencies the change in current due to a small deviation in rotation speed ω will produce a change in torque that increases the original deviation in ω. This effect was caused by the fact that the magnet, which produces a constant field, views the rest of the motor as an induction machine. The braking torque due to the current caused by the emf shows a similar frequency dependence to the induction machine.

Other synchronous machines that are driven in open loop such as turbo generators in power plants would also experience instability if no measures were taken. To counter that instability those generators are fitted with damping cages, which dampen any oscillations that are superimposed on the synchronous rotation of the generator but do not effect the steady state rotation itself. These damper cages suppress all frequencies other than the synchronous frequency, and as such have an important function in offering protection against disturbances on the net.

This section aims to implement a controller that has the same goal as the damping cage: to dampen oscillations superimposed on the steady state rotation whilest not dissipating energy when the motor is in steady state.

Since it is not possible to fit already existing stepper motors with damping cages, the approach chosen is to mimic a damping cage. The phase currents are measured, and these are used to control the phase input voltage amplitude and phase. When an oscillation occurs in the motor the controller will manipulate the input voltage vector such that energy is dissipated from the oscillation but not from steady state rotation just like a damping cage would do.

3.1. The Ideal Rotating TransFormer

To implement the model of (3) the currents in the motor have to be modeled in (d,q) coordinates, while the phase voltages are applied at the stator side in (α,β) coordinates. The Ideal Rotating TransFormer (IRTF) [7] is a tool that separates the motor into three domains; the stator-, the rotor- and the mechanical domain. The IRTF allows power to move between these domains but it does not dissipate any power itself, nor does it store any energy.. Schematically a motor model using an IRTF is shown in figure 14.

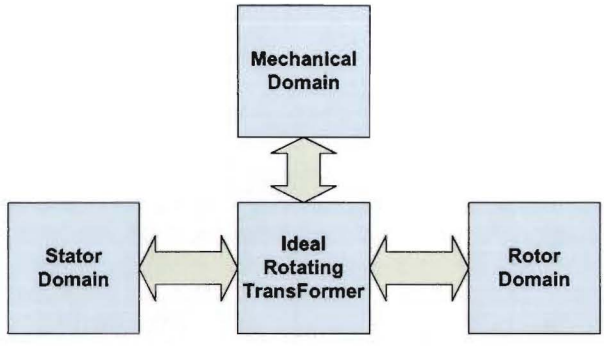

Fig. 14. Block diagram of a model using an Ideal Rotating TransFormer. Note that the IRTF itself has no internal states and does not dissipate energy.

An IRTF model represents the current flowing in the motor phases as a vector which can be viewed in different coordinate systems. The IRTF rotates the vector of current in the motor between stator and rotor coordinates over the absolute rotor

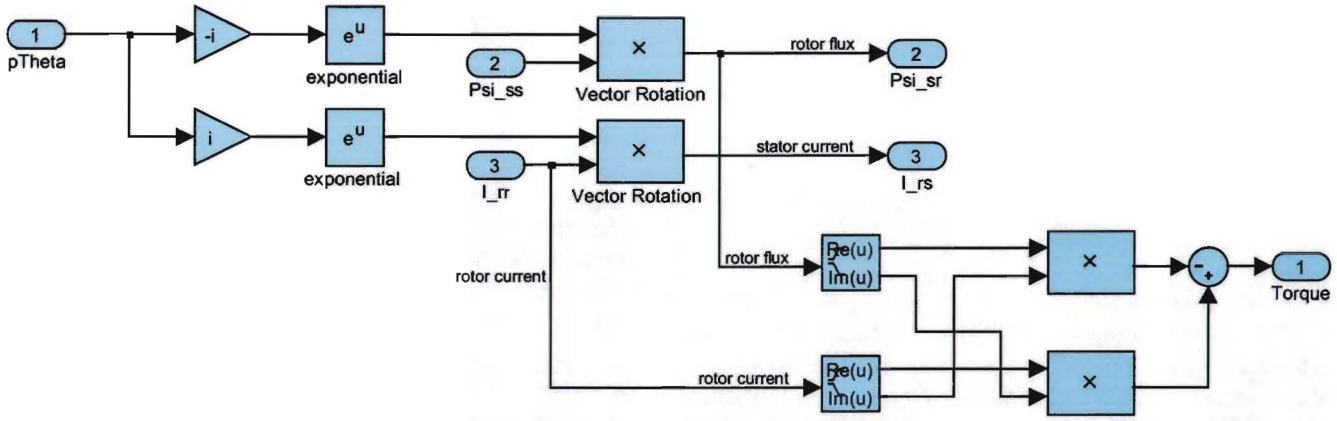

Fig. 12. Simulink implementation of an Ideal Rotating TransFormer. The current- and flux vectors are rotated over angles of $\pm p\theta$ by multiplying them with $e^{\mp p\theta}$. The produced torque is given by taking the cross product of the rotor flux vector and the rotor current vector.

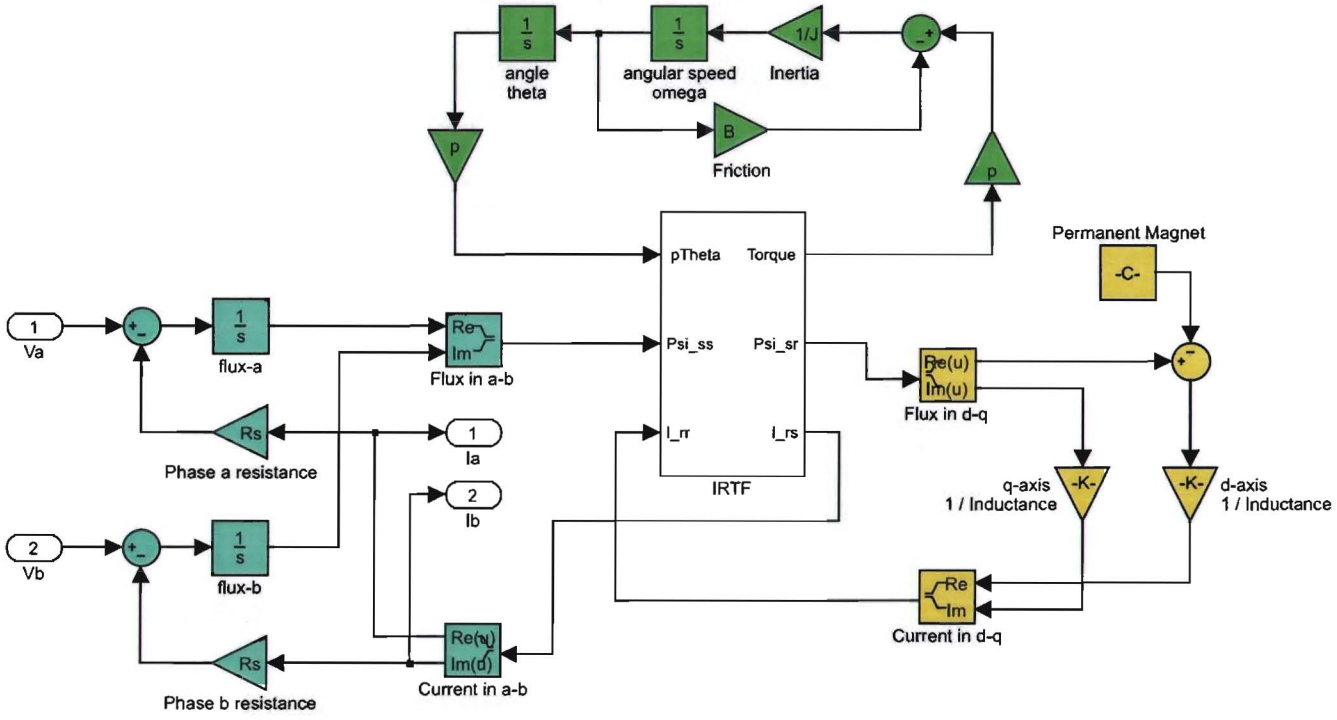

Fig. 13. Implementation of stepper motor model (3) using an IRTF in Simulink. The stator side is shown on the left, the rotor side on the right and the mechanical part is represented by the green part in the top.

angle $p\theta$. It does the same with the vector of motor flux. In the version of the IRTF used the stator produces the flux, which is rotated to rotor coordinates. The rotor produces a current from the input flux which is then transformed back into stator coordinates. If the angle between the current and torque vectors is not equal to zero, the motor produces torque. The torque is then given by viewing the part of the current vector that is perpendicular to the flux vector. Mathematically the torque is given by the cross product between the torque and current vectors. The simulink model of the IRTF used is shown in figure 12.

The IRTF enables seperate modeling of the stator and the rotor. In the case of the model of (3) the total model consists of two phases with a resistance, an inductance and a source of emf. This can be implemented using the IRTF by representing the stator phases with a resistance, and the rotor with inductances. The permanent magnet is modeled by a fixed source of flux in the direction of the d-axis on the rotor. Modeling the stepper motor in this way results in a Simulink model as shown in figure 13.

It is very important to realize that the model of figure 13 is mathematically equivalent to the model of (3). The proof of equivalence can be found in appendix IV. Modeling of the stepper motor using an IRTF has some key advantages:

- All the states are directly visible and accessible, which gives insight in the system behaviour. Also the flux in the

motor can be viewed/altered directly.
- The stator and the rotor are seperately modeled. This means that effects can be modeled in the place where they actually physically occur. For instance reluctance effects and magnet emf can be modeled on the rotor side.
- The model is valid for any input waveform and any type of rotor movement, so also out of sync behaviour can be analysed.

3.2. Controller structure

The controller proposed in this paper tries to mimic the damping cage. When oscillation occur in the movement of the rotor the controller adjusts the voltage to counter effect the oscillation. Schematically the controller is shown in the figure 16.

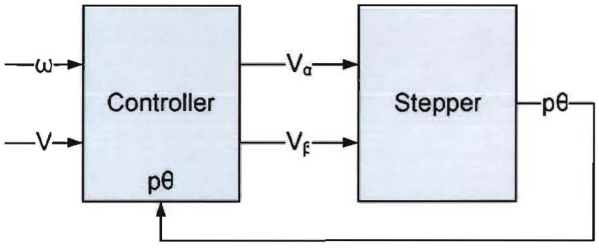

Fig. 16. Block diagram of stepper motor with controller. The controller outputs the phase voltages to the stepper motor, and uses the rotor angle to detect oscillations superimposed on the synchronous frequency. When there are oscillations it adepts the voltage to dampen these oscillations.

The controller steers the phase voltages that are inputs to the motor. In steady state rotation the input voltage is a rotating vector. When the angle of the rotor is greater than it should be in steady state the controller scales down the voltage. This will cause the rotor to move back towards the steady state rotation, and removes energy from oscillations superimposed on the steady state rotation.

The controller subtracts the actual rotor angle from the steady state rotor angle. The resulting difference angle is filtered with a second order high pass filter which has a cutoff frequency at 10 Hz. Any oscillations are assumed to have a higher frequency than 10 Hz, since the oscillations that are associated with instability are at the motors natural frequency. If any oscillations are present the controller makes a ΔV which is added to the amplitude of the input voltage vector. The ΔV is always in the direction to counter the oscillation causing it. The controller implementation is shown in figure 15.

Note that to implement this controller the rotor angle needs to be known to the controller. Since the only information that is known are the phase currents and voltages, the exact rotor angle is not known. However, an approximate angle can be computed from the known signals using and observer, as described in the next section.

Since the proposed controller is completely linear, it can be included in the system equations. Because the high pass filter has two states, the system including the controller will be of the sixth order. The extra states introduced by the high pass filter are named H_1 and H_2. Another two variables are introduced by the controller, namely the cutoff frequency of the highpass filter A and the controller gain K. The system including the controller is given by (13). Note that $\Delta V = K(p\omega_s t - p\theta - H_1 - H_2)$, and that ω_s is the applied source frequency.

The controller is tested by speeding up the K223 stepper motor, both for the motor without controller and for the motor including the controller. During the experiment a 5 Hz square wave disturbance torque of 10% of the nominal motor torque. The responses for the open loop and the controlled system are shown in figure 17.

3.3. Speed and angle observer

To control the stepper motor reliably information about the actual stepper motor angle and speed is very useful. The only information available when an encoder is not used are the phase voltages and the phase currents. Multiple attempts have been made at estimating the rotor position and speed from these available signals [13], [15], [14], [10]. The solution proposed by Yang in [10], which uses a Phase Locked Loop (PLL) is the most recent contribution and is the most suitable in this application. The observer implementation in Simulink is shown in figure 18.

The observer measures the emf voltage and uses this voltage to lock a PLL resulting in an estimation for angle and angular speed of the motor. Rewriting 2 to isolate the emf voltage we have:

$$\begin{aligned}\begin{pmatrix} V_{emf\_\alpha} \\ V_{emf\_\beta} \end{pmatrix} &= \begin{pmatrix} p\lambda_m \sin(p\theta)\omega \\ -p\lambda_m \cos(p\theta)\omega \end{pmatrix} \\ &= \begin{pmatrix} -R - L\frac{di_\alpha}{dt} & 0 \\ 0 & -R - L\frac{di_\beta}{dt} \end{pmatrix} \begin{pmatrix} i_\alpha \\ i_\beta \end{pmatrix} \\ &\quad + \begin{pmatrix} v_\alpha \\ v_\beta \end{pmatrix}\end{aligned} \tag{14}$$

For positive angular speed ω the current in phase α will be 90 degrees ahead of the current in phase β, such that for some A and ϕ the phase currents can be described by:

$$\begin{aligned} i_\alpha &= A\cos(p\omega t + \phi) \\ i_\beta &= A\sin(p\omega t + \phi) \end{aligned}$$

Because the phase currents are harmonic functions of the same frequency $p\omega$ their derivatives can be written as a function of the phase currents themselves:

$$\begin{aligned} \frac{di_\alpha}{dt} &= -A\sin(p\omega t + \phi)p\omega = -p\omega i_\beta \\ \frac{di_\beta}{dt} &= A\cos(p\omega t + \phi)p\omega = p\omega i_\alpha \end{aligned} \tag{15}$$

Combining (15) with (14) gives an expression for the emf voltage which depends solely on directly available voltages and currents, and the applied frequency ω which is also available. The result from combining the equations is:

$$\begin{pmatrix} V_{emf\_\alpha} \\ V_{emf\_\beta} \end{pmatrix} = \begin{pmatrix} -R & p\omega L \\ -p\omega L & -R \end{pmatrix} \begin{pmatrix} i_\alpha \\ i_\beta \end{pmatrix} + \begin{pmatrix} v_\alpha \\ v_\beta \end{pmatrix} \tag{16}$$

The implementation of this emf calculation is shown in the left part of figure 18. The emf voltages are used to obtain an

$$\frac{d}{dt}\begin{pmatrix} i_d \\ i_q \\ \omega \\ \theta \\ H_1 \\ H_2 \end{pmatrix} = \begin{pmatrix} \frac{-R}{L} & p\omega & 0 & 0 & 0 & 0 \\ -p\omega & \frac{-R}{L} & \frac{-p\lambda_m}{L} & 0 & 0 & 0 \\ 0 & \frac{p\lambda_m}{J} & \frac{-B}{J} & 0 & 0 & 0 \\ 0 & 0 & 1 & 0 & 0 & 0 \\ 0 & 0 & 0 & -pA & -A & 0 \\ 0 & 0 & 0 & -pA & -A & -A \end{pmatrix} \begin{pmatrix} i_d \\ i_q \\ \omega \\ \theta \\ H_1 \\ H_2 \end{pmatrix} + \begin{pmatrix} \frac{(V+\Delta V)\cos(p\omega_s - p\theta)}{L} \\ \frac{(V+\Delta V)\sin(p\omega_s - p\theta)}{L} \\ \frac{-T_l}{J} \\ 0 \\ Ap\omega_s t \\ Ap\omega_s t \end{pmatrix} \tag{13}$$

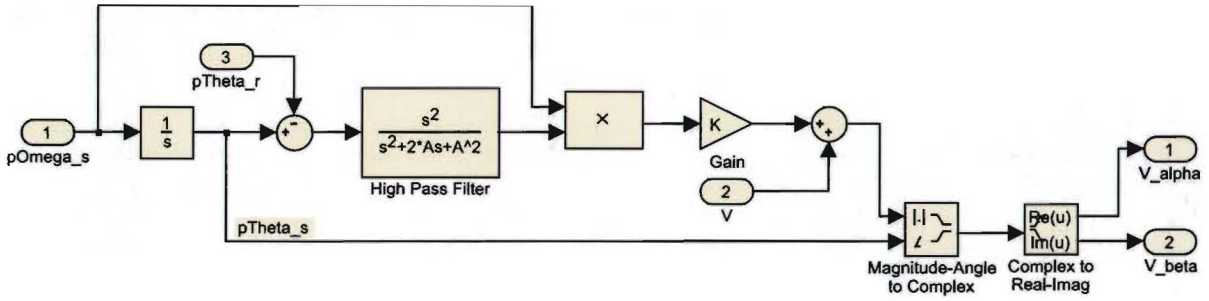

Fig. 15. Simulink implementation of the controller. Inputs are stator frequency $p\omega_s$, nominal voltage V, and the actual rotor angle $p\theta$. The controller adjusts the amplitude of the voltage vector to dampen oscillations on the rotor angle.

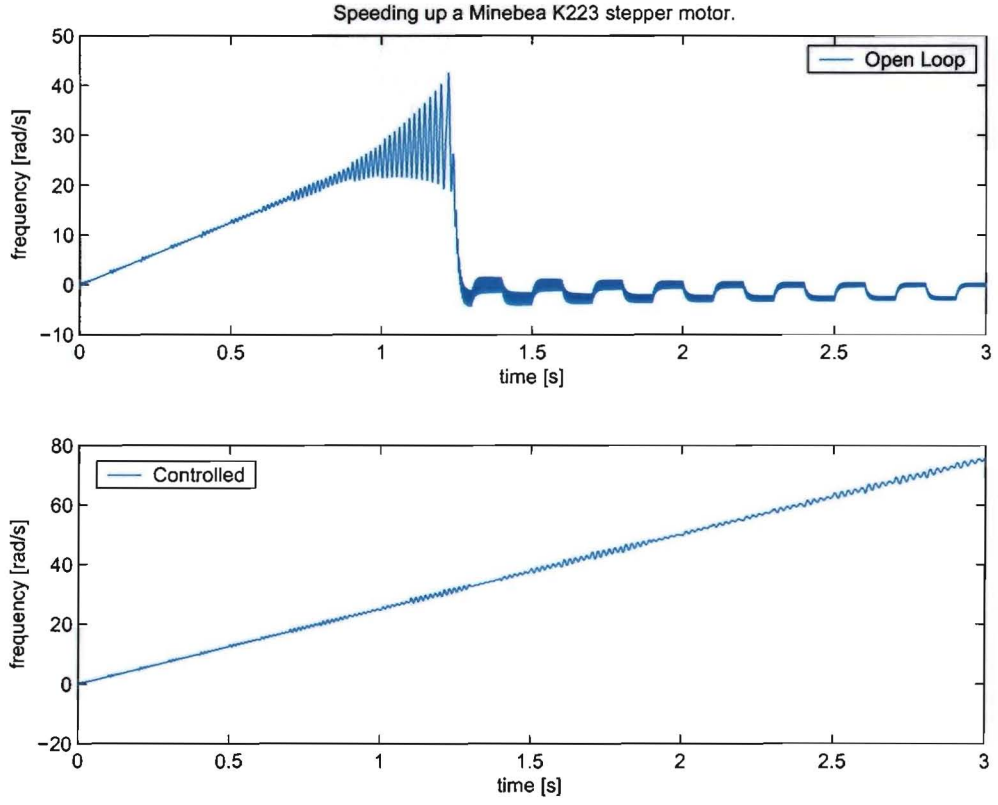

Fig. 17. Simulated response of Minebea K223 when increasing rotation speed. The open loop system is clearly unstable, while the controlled system does not suffer from the instability at all. During the experiment the motor is subjected to a 5 Hz square wave disturbance torque of 10% of the maximum motor torque.

estimate for the motor angle $\hat{p\theta} = p\theta + p\theta_{err}$. This is achieved by multiplying them with the cosine (or sine) of the estimate angle and adding them together in the following manner:

$$\begin{aligned} & V_{emf\_\alpha}\cos(\hat{p\theta}) + V_{emf\_\beta}\sin(\hat{p\theta}) \\ &= p\lambda_m \sin(p\theta)\omega\cos(p\theta + p\theta_{err}) \\ &\quad -p\lambda_m \cos(p\theta)\omega\sin(p\theta + p\theta_{err}) \\ &= -p\lambda_m\omega\sin(p\theta_{err}) \\ &\approx -p\lambda_m\omega p\theta_{err} \end{aligned}$$

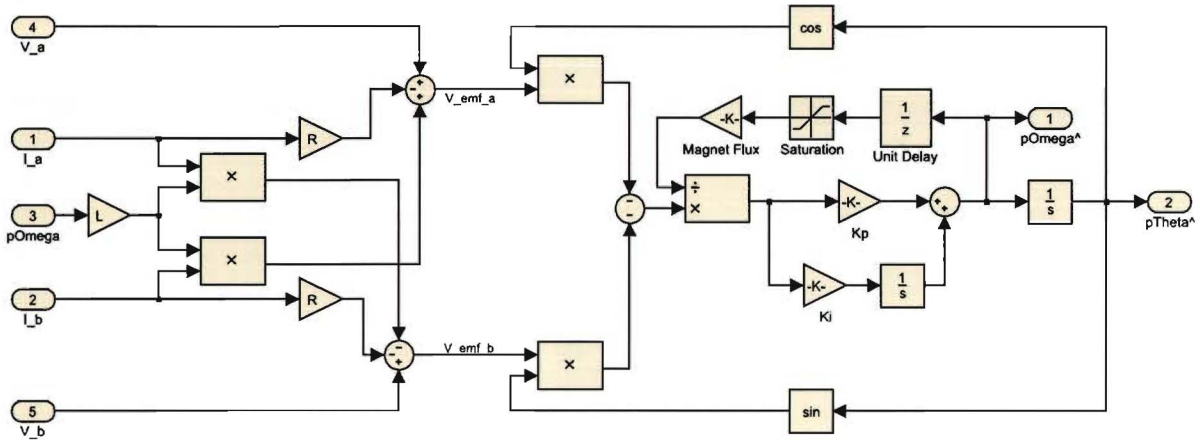

Fig. 18. Simulink model of the rotor angle and speed observer. The observer first calculates the emf voltages from the phase voltages and the phase currents. The information contained in the emf about rotor angle is used as input for a phase locked loop (PLL), which tracks the rotor angle and speed.

This result is divided by $p\lambda_m p\omega$ such that only the error angle θ_{err} is left. The PI controller with the feedback through the multiplication with the sine/cosine of the estimated angle will force the error angle θ_{err} to zero. The transfer function from angle to estimated angle becomes:

$$\begin{aligned} p\hat{\omega} &= (K_p + \frac{K_i}{s}) p\theta_{err} \\ &= (K_p + \frac{K_i}{s})(\frac{p\omega}{s} - \frac{p\hat{\omega}}{s}) \\ \frac{p\hat{\omega}}{p\omega} &= \frac{K_p s + K_i}{s^2 + K_p s + K_i} \end{aligned}$$

By selecting values for K_p and K_i the observer poles can be placed at will. Selecting proper values will assure good tracking of the rotor frequency and angle. In simulations, good tracking was achieved using $K_p = 1000$, $K_i = 5000$. The tracking of the observer is shown in figure 19.

3.4. Other ways to control the stepper motor

Of course, the proposed method is not the only way to stabilise hybrid stepper motors. If the observer tracking were perfect then all states would be observable, and there is a lot of freedom in placing the eigenvalues of the total system. For example a normal servo controller can be implemented [10]. A similar option is presented in [11]. Other publications describing control algorithms are described in [13], [15], [17], [18].

4. Conclusions & Recommendations

Hybrid stepper motors are widely used, even though most users do not fully understand their dynamics. Most research into stepper motor theory was done before 1985, and the common driving principles were developed in those days. Since then computing power has become a lot cheaper, to the point where small microprocessors are now less costly evn than encoder wheels. This effect has greatly extended the posibilities for stepper motor operation. Complex waveform drivers, and current sensing applications are now available at low costs.

However, most stepper motor users still work with full-step current chopping drivers. The main disadvantages of this technique are power inefficiency and excessive noise generation. Especially at low frequencies a lot of power is wasted by employing full-step current driving. To make the switch to more complicated ways of driving stepper motors profound knowledge about the motor dynamics is needed. Since this is not available to most users and ready made solutions so far remain absent it may still take some time before novel driving techniques find their way to mainstream users.

In this paper the instability in stepper motors was shown to be caused by the braking torque which results from the current produced by the emf. The derivative of the this torque with respect to rotation frequency ω was shown to be positive for all frequencies greater than $p\omega = \frac{R}{L}$. For all those frequencies the emf braking torque exerts a destabilising effect on the motor. If the motor actually becomes unstable was shown to depend on viscous damping B and rotating inertia J.

Stability conditions are formulated that allow to predict exactly for what frequency the instability will occur, both for motors with and for motors without viscous damping. The instability is shown to start at $p\omega = \frac{R}{L}$ when there is no damping and the inertia is large enough. For motors with smaller inertias the instability was shown to start at higher frequency. The viscous damping term B was shown to have a stabilising effect on the motor at all times, and for any value of B the stability condition can be plotted showing for which frequencies to expect instability.

A controller was designed and implemented in Simulink for the K223 stepper motor. The proposed controller adjusts the source voltage when it detects the motor is not in steady state. In simulations the motor which is unstable in open loop is stabilised by the proposed controller. The controller uses an observer which tracks the rotor load angle and angular speed from the phase voltages and currents. The observer was also implemented in Simulink, and showed good tracking for

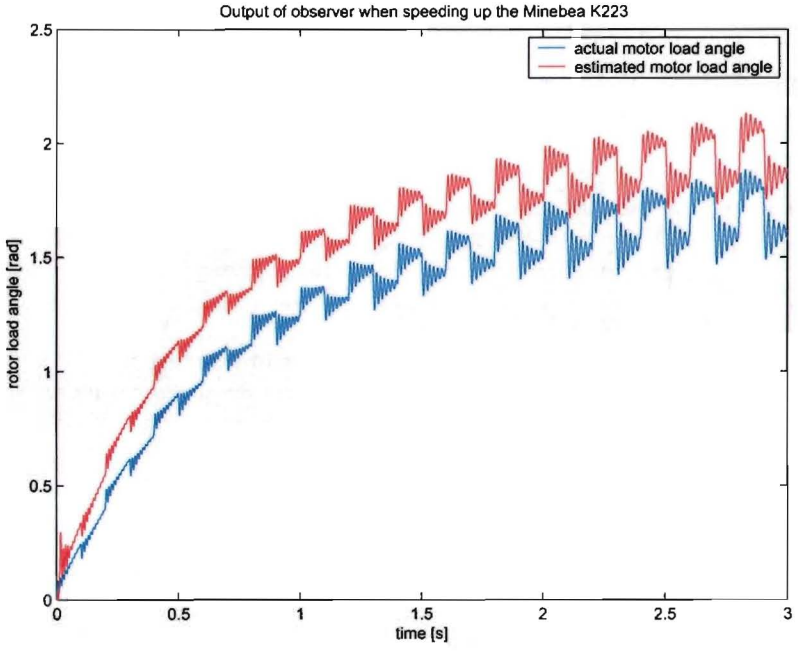

Fig. 19. Tracking of the observer during the speeding up of the Minebea K223 experiment. Although there is a steady state tracking error, the high frequency behaviour of the observer is quite good. For very low frequencies the observer does not function very well due to the lack of emf voltage.

higher frequencies.

Future research in this project could be to implement the controller into the actual setup. Unfortunately the implementation could not be finished in time to include it in this report. Although the nonlinear simulations suggest the results which were obtained by linearisation are correct, measurements would have to be done to verify the instability conditions and the correct functioning of the controller and observer. Also it would be valuable to compare the prestations of the proposed controller with other controllers both in simulation and in the actual setup.

Because the equations become rather cumbersome, an analytical proof of stability for the controller is currently not presented. That is still an open question, as is rewriting the strongly nonlinear stability criteria to isolate frequency ω. If ω could be isolated an analytical expression for the instability frequency would be available, and the stability threshhold would not have to be deduced from a graph of the criterion.

REFERENCES

[1] A. Hughes and P.J. Lawrenson, *Simple theoretical stability criteria for 1.8° hybrid motors*, proc. int. symp. on stepping motors and systems; University of Leeds, 1979, pp 127-135

[2] A. Hughes, P.J. Lawrenson and T.S. Davies, *Factors determining high-speed torque in hybrid motors*, In Proc. Int. Symp. on Stepping Motors and System; University of Leeds, 1976, pp 150-157

[3] G.C. Verghese, J.H. Lang and L.F. Casey, *Analysis of electric instability in electrical machines*, IEEE Trans on Industry Applications, 22(5), 1986, pp 853-864

[4] A. Hughes and P.J. Lawrenson, *Electromagnetic damping in stepping motors*, Proceedings IEE, 122(8), 1975, pp 819-824

[5] I.E.D. Pickup and A.P. Russel, *Dynamic instability in permanent-magnet synchronous/stepping motors*, Proceedings IEE, 134(B2), 1987, pp 91-100

[6] P.J. Lawrenson and I.E. Kingham, *Resonance effects in stepping motors*, Proceedings IEE, 124(5), 1977, pp 445-448

[7] A. Veltman and P.P.J. van den Bosch, *A universal method for modelling electrical machines*, In Proc. Conf. on Electrical Machines and Drives, 1992, pp 193-197

[8] P.P. Acarnley, *Stepping Motors, a guide to theory and practice*, London: The Institution of Electrical Engineers (IEE), 2002, 4th edition

[9] P.J. Clarkson and P.P. Acarnley, *Stability limits for dynamic operation of variable reluctance stepping motor systems*, In Proc. Conf. on Electrical Power Applications, 1988, pp 308-317

[10] S-M. Yang and E-L. Kuo, *Dampin a hybrid stepper motor with estimated position and velocity*, IEEE Transactions on Power Electronics, 18(3), 2003, pp 880-887

[11] K. Mizutani, S. Hayshi and N. Matsui, *Modeling and control of hybrid stepping motors*, In IEEE Conf. Record on Industrial Applications and Systems, vol. 1, 1993, pp 289-294

[12] C. Kuert, M. Jufer and Y. Perriard, *New method for dynamic modeling of hybrid stepping motors*, In IEEE Conf. Record on Industry Applications and Systems, vol. 1, 2002, pp 6-12

[13] P.P. Acarnley, R.J. Hill and C.W. Hooper, *Detection of rotor position in stepping and switched motors by monitoring of current waveforms*, IEEE Transactions on Industrial Electronics, 32(3), 1985, pp 215-222

[14] A. Imagi, M. Tomisawa and T. Koizumi, *State and parameter estimation for step motors under actual working conditions*, 16th Annual Conference IEEE Industrial Electronics Society, 1990, pp 114-119

[15] S.A. Schweid et al, *Hybrid step motor position estimation fro back EMF*, In Proc. IEEE Conf. on Control Applications, 1995, pp 774-778

[16] P.A. Ward and P.J. Lawrenson, *Backlash, resonance and instability in stepping motors*, In Proc. 6th Annual Symp. on Incremental Motion Control Systems and Devices, 1977, pp 73-83

[17] P.J. Clarkson and P.P. Acarnley, *Closed-loop control of stepping motor systems*, IEEE Transactions on Industry Applications, 24(4), 1988, pp 685-691

[18] J.B. Grimbleby, *Simple algorithm for closed-loop control of stepping motors*, Proceedings IEE EPA, 142(1), 1995, pp 5-13

[19] A.M. Harb and A.A. Zaher, *Nonlinear control of permanent magnet stepper motors*, Journal on Commununications in Nonlinear Science and Numerical Simulation, 9, 2004, pp 443-458

[20] M. Zribi and J. Chiasson, *Position control of a PM stepper motor by exact linearization*, IEEE Transactions on Automatic Control, 36(5), 1991, pp 620-625

[21] B.H.A. Goddijn, *Analog electronic damping of stepping motors*, In Proc. Int. Symp. on Stepper Motors and Systems, 1976, pp 61-67

APPENDIX I
CALCULATING THE OPERATING POINT

This appendix shows the calculation of the steady state operating point for the stepper motor based on the model presented earlier as (6), which is restated here as (17). In this system the load torque T_l and the rotation frequency ω considered input variables.

$$\frac{d}{dt}\begin{pmatrix} i_d \\ i_q \\ \omega \\ \theta \end{pmatrix} = \begin{pmatrix} -R/L & p\omega & 0 & 0 \\ -p\omega & -R/L & -p\lambda_m/L & 0 \\ 0 & p\lambda_m/J & -B/J & 0 \\ 0 & 0 & 1 & 0 \end{pmatrix}\begin{pmatrix} i_d \\ i_q \\ \omega \\ \theta \end{pmatrix} + \begin{pmatrix} V\cos(\delta)/L \\ V\sin(\delta)/L \\ -T_l/J \\ 0 \end{pmatrix} \tag{17}$$

From this system of equations the steady state solution can be calculated by putting $\frac{di_d}{dt} = \frac{di_q}{dt} = \frac{d\omega}{dt} = \frac{d\theta}{dt} = 0$, and finding the values for i_d, i_q and δ that satisfy the resulting equations. Looking at the equation resulting from putting $\frac{di_d}{dt} = 0$ results in an intermedate solution for i_d and δ given in (18):

$$\begin{aligned} \frac{di_d}{dt} = 0 &= -\frac{R}{L}i_d + \frac{V}{L}\cos(\delta) + p\omega i_q \\ i_d &= \frac{p\omega L}{R}i_q + \frac{V}{R}\cos(\delta) \end{aligned} \tag{18}$$

The intermediate result from (18) can be used to find an intermediate result for i_q and δ from the equation associated with putting $\frac{di_q}{dt} = 0$.

$$\begin{aligned} \frac{di_q}{dt} &= -\frac{p^2\omega^2 L}{R}i_q - \frac{p\omega V}{R}\cos(\delta) - \frac{R}{L}i_q - \frac{p\lambda_m}{L}\omega + \frac{V}{L}\sin(\delta) \\ 0 &= p^2\omega^2 L^2 i_q - p\omega LV\cos(\delta) - R^2 i_q - p\lambda_m R\omega \end{aligned}$$

Rearranging to isolate i_q:

$$\begin{aligned} i_q(R^2 + p^2\omega^2 L^2) &= V(R\sin(\delta) - p\omega L\cos(\delta)) - p\lambda_m R\omega \\ i_q &= \frac{V}{R^2 + p^2\omega^2 L^2}(R\sin(\delta) - p\omega L\cos(\delta)) - \frac{p\lambda_m\omega R}{R^2 + p^2\omega^2 L^2} \end{aligned} \tag{19}$$

Closer inspection of (19) shows that the relation between i_q and δ is determined by both a sine and a cosine function. These two functions can be combined to form one single harmonic function as shown below:

$$\begin{aligned} R\sin(\delta) - p\omega L\cos(\delta) &= R\left(\frac{e^{j\delta} - e^{-j\delta}}{2j}\right) - p\omega L\left(\frac{e^{j\delta} + e^{-j\delta}}{2}\right) \\ &= R\left(\frac{e^{j\delta} - e^{-j\delta}}{2j}\right) - jp\omega L\left(\frac{e^{j\delta} + e^{-j\delta}}{2j}\right) \\ &= \frac{(R - jp\omega L)e^{j\delta} - (R + jp\omega L)e^{-j\delta}}{2j} \\ &= \sqrt{R^2 + p^2\omega^2 L^2}\left(\frac{e^{j(\delta-\phi_o)} - e^{-j(\delta-\phi_o)}}{2j}\right) \\ &= \sqrt{R^2 + p^2\omega^2 L^2}\sin(\delta - \phi_o) \end{aligned} \tag{20}$$

In the above expression the offset angle ϕ_o is introduced, which is described by $\phi_o = \arctan\left(\frac{p\omega L}{R}\right)$. This offset angle is caused by the complex phase impedance and not by any load in the system. Substituting the above result in the intermediate expression for i_q and δ yields a new intermediate expression as shown in (21):

$$\begin{aligned} i_q &= \frac{V\sqrt{R^2 + p^2\omega^2 L^2}}{R^2 + p^2\omega^2 L^2}\sin(\delta - \phi_o) - \frac{p\lambda_m\omega R}{R^2 + p^2\omega^2 L^2} \\ &= \frac{V}{\sqrt{R^2 + p^2\omega^2 L^2}}\sin(\delta - \phi_o) - \frac{p\lambda_m\omega R}{R^2 + p^2\omega^2 L^2} \end{aligned} \tag{21}$$

Examining the equation for $\frac{d\omega}{dt}$ directly gives a simple equation for i_q:

$$\begin{aligned} \frac{d\omega}{dt} &= \frac{p\lambda_m}{J} i_q - \frac{B\omega}{J} - \frac{T_l}{J} \\ 0 &= p\lambda_m i_q - B\omega - T_l \\ i_q &= \frac{B\omega + T_l}{p\lambda_m} \end{aligned} \tag{22}$$

Now there are two equations for i_q in steady state, one of which is dependent of δ. This means that by combining (21) with (22) the operating point for the load angle δ can be calculated.

$$\begin{aligned} \frac{V}{\sqrt{R^2+p^2\omega^2L^2}} \sin(\delta - \phi_o) - \frac{p\lambda_m \omega R}{R^2+p^2\omega^2L^2} &= \frac{B\omega+T_l}{p\lambda_m} \\ \frac{V}{\sqrt{R^2+p^2\omega^2L^2}} \sin(\delta - \phi_o) &= \frac{B\omega+T_l}{p\lambda_m} + \frac{p\lambda_m \omega R}{R^2+p^2\omega^2L^2} \\ \sin(\delta - \phi_o) &= \frac{(B\omega+T_l)\sqrt{R^2+p^2\omega^2L^2}}{p\lambda_m V} + \frac{p\lambda_m \omega R}{V\sqrt{R^2+p^2\omega^2L^2}} \\ \delta &= \arcsin\left(\frac{(B\omega+T_l)\sqrt{R^2+p^2\omega^2L^2}}{p\lambda_m V} + \frac{p\lambda_m \omega R}{V\sqrt{R^2+p^2\omega^2L^2}}\right) + \phi_o \end{aligned}$$

So the load angle consists of an offset part given by the arctangent and a load part. In the load part of the angle again two different effects can be noticed. The first term in the arcsine is due to load torque and friction, while the second is to overcome the braking effect of the emf.

The operating point for i_d is best calculated from the intermediate result (18) because filling in the values for δ and i_q only gives a very long equation that cannot be simplified. So summarizing the operating points for steady state rotation are given by:

$$i_q = \frac{B\omega + T_l}{p\lambda_m} \tag{23a}$$

$$\delta = \arcsin\left(\frac{(B\omega + T_l)\sqrt{R^2 + p^2\omega^2L^2}}{p\lambda_m V} + \frac{p\lambda_m \omega R}{V\sqrt{R^2 + p^2\omega^2L^2}}\right) + \phi_o \tag{23b}$$

$$i_d = \frac{p\omega L}{R} i_q + \frac{V}{R}\cos(\delta) \tag{23c}$$

APPENDIX II
CALCULATION OF THE POINT OF INSTABILITY

In this appendix the frequency at which the motor first becomes unstable is calculated. To this end the eigenvalues of the linearised system matrix are examined analytically, by making use of the Routh-Hurwitz theorem. The resulting stability criteria are analysed and it is shown the motor stability depends on only one of them. Finally, an analytical expression for the point of instability is formulated.

View the linearised system equations of (9) which are restated here as (24) for clarity.

$$\frac{d}{dt}\begin{bmatrix}\delta i_d\\ \delta i_q\\ \delta\omega\\ \delta\theta\end{bmatrix} = \begin{bmatrix}-R/L & p\omega & pi_q & pV sin(\delta)/L\\ -p\omega & -R/L & -(pi_d + p\lambda_m/L) & -pV cos(\delta)/L\\ 0 & p\lambda_m/J & -B/J & 0\\ 0 & 0 & 1 & 0\end{bmatrix}\begin{bmatrix}\delta i_d\\ \delta i_q\\ \delta\omega\\ \delta\theta\end{bmatrix} \tag{24}$$

The system becomes unstable when at least one of the eigenvalues of the matrix has positive real value. The eigenvalues of the matrix are given by solving $det(sI - A) = 0$ for s.

$$\begin{aligned}
|sI - A| &= \left|\begin{pmatrix}s&0&0&0\\0&s&0&0\\0&0&s&0\\0&0&0&s\end{pmatrix} - \begin{pmatrix}-R/L & p\omega & pi_q & pV\sin(\delta)/L\\ p\omega & -R/L & -(pi_d + p\lambda_m/L) & -pV\cos(\delta)/L\\ 0 & p\lambda_m/J & -B/J & 0\\ 0 & 0 & 1 & 0\end{pmatrix}\right|\\
&= \begin{vmatrix} s + R/L & -p\omega & -pi_q & -pV\sin(\delta)/L\\ p\omega & s + R/L & pi_d + p\lambda_m/L & pV\cos(\delta)/L\\ 0 & -p\lambda_m/J & s + B/J & 0\\ 0 & 0 & -1 & s\end{vmatrix}\\
&= s^4 + (\frac{B}{J} + 2\frac{R}{L})s^3 + (2\frac{R}{L}\frac{B}{J} + \frac{p\lambda_m}{J}(pi_d + \frac{p\lambda_m}{L}) + (\frac{R^2}{L^2} + p^2\omega^2))s^2\\
&\quad +(\frac{B}{J}(\frac{R^2}{L^2} + p^2\omega^2)) + \frac{R}{L}\frac{p\lambda_m}{J}(pi_d + \frac{p\lambda_m}{L}) + \frac{p\lambda_m}{J}(p\omega pi_q + \frac{pV\cos(\delta)}{L}))s +\\
&\quad (\frac{R}{L}\frac{p\lambda_m}{J}\frac{pV\cos(\delta)}{L} + p\omega\frac{p\lambda_m}{J}\frac{pV\sin(\delta)}{L})\\
&= as^4 + bs^3 + cs^2 + ds + e
\end{aligned}$$

where

$$\begin{aligned}
a &= 1\\
b &= \tfrac{B}{J} + 2\tfrac{R}{L}\\
c &= 2\tfrac{R}{L}\tfrac{B}{J} + \tfrac{p\lambda_m}{J}(pi_d + \tfrac{p\lambda_m}{L}) + (\tfrac{R^2}{L^2} + p^2\omega^2)\\
d &= \tfrac{B}{J}(\tfrac{R^2}{L^2} + p^2\omega^2)) + \tfrac{R}{L}\tfrac{p\lambda_m}{J}(pi_d + \tfrac{p\lambda_m}{L}) + \tfrac{p\lambda_m}{J}(p\omega pi_q + \tfrac{pV\cos(\delta)}{L})\\
e &= \tfrac{R}{L}\tfrac{p\lambda_m}{J}\tfrac{pV\cos(\delta)}{L} + p\omega\tfrac{p\lambda_m}{J}\tfrac{pV\sin(\delta)}{L}
\end{aligned} \tag{25}$$

According to the Routh-Hurwitz theorem the solutions to $s^4 + bs^3 + cs^2 + ds + e = 0$ have negative real parts if:

$$\Delta_1 > 0, \Delta_2 > 0, \Delta_3 > 0, \Delta_4 > 0 \tag{26}$$

where

$$\begin{aligned}
\Delta_1 &= |b|\\
&= b\\
\Delta_2 &= \begin{vmatrix} b & 1\\ d & c\end{vmatrix}\\
&= bc - d\\
\Delta_3 &= \begin{vmatrix} b & 1 & 0\\ d & c & b\\ 0 & e & d\end{vmatrix}\\
&= bcd - d^2 - eb^2\\
\Delta_4 &= \begin{vmatrix} b & 1 & 0 & 0\\ d & c & b & 1\\ 0 & e & d & c\\ 0 & 0 & 0 & e\end{vmatrix}
\end{aligned}$$

$$\begin{aligned} &= bcde - d^2e - b^2e^2 \\ &= e\Delta_3 \end{aligned}$$

Due to the number of arguments the computation of the exact instability is rather complex. If it is assumed that the damping parameter B which is always positive or zero contributes in a stabilising manner the worst case stability would be at $B = 0$. This assumption can be justified by the fact that the damping will always dissipate energy from any oscillation. Also, the observation made in section 2 that the root locus is shifted towards the left halfplane by increasing the damping B supports this assumption. If the damping parameter B is set to zero, the characteristic polynomial factors of (25) reduce to:

$$\begin{aligned} a &= 1 \\ b &= 2\tfrac{R}{L} \\ c &= \tfrac{p\lambda_m}{J}(pi_d + \tfrac{p\lambda_m}{L}) + (\tfrac{R^2}{L^2} + p^2\omega^2) \\ d &= \tfrac{R}{L}\tfrac{p\lambda_m}{J}(pi_d + \tfrac{p\lambda_m}{L}) + \tfrac{p\lambda_m}{J}(p\omega pi_q + \tfrac{pV\cos(\delta)}{L}) \\ e &= \tfrac{R}{L}\tfrac{p\lambda_m}{J}\tfrac{pV\cos(\delta)}{L} + p\omega\tfrac{p\lambda_m}{J}\tfrac{pV\sin(\delta)}{L} \end{aligned} \tag{27}$$

Note that since the system starts in steady state $pi_d = \frac{p\omega L}{R}pi_q + \frac{pV}{R}\cos(\delta)$. This equality can be used to further simplify d in (27):

$$\begin{aligned} d &= \frac{R}{L}\frac{p\lambda_m}{J}(pi_d + \frac{p\lambda_m}{L}) + \frac{p\lambda_m}{J}(p\omega pi_q + \frac{pV\cos(\delta)}{L}) \\ &= \frac{R}{L}\frac{p\lambda_m}{J}(pi_d + \frac{p\lambda_m}{L}) + \frac{p\lambda_m}{J}(\frac{R}{L}pi_d) \\ &= \frac{R}{L}\frac{p\lambda_m}{J}(2pi_d + \frac{p\lambda_m}{L}) \end{aligned}$$

Using these parameters the stability criteria of (26) can be examined.

$$\begin{aligned} \Delta_1 &> 0 \\ b &> 0 \\ 2\frac{R}{L} &> 0 \end{aligned}$$

This criterion is always satisfied for positive phase resistance R and inductance L. Since R and L are positive in any stepper motor this stability criterion is always satisfied. The second criterion gives:

$$\begin{aligned} \Delta_2 &> 0 \\ bc - d &> 0 \\ 2\frac{R}{L}((\frac{R^2}{L^2} + p^2\omega^2) + \frac{p\lambda_m}{J}(pi_d + \frac{p\lambda_m}{L})) - \frac{R}{L}\frac{p\lambda_m}{J}(2pi_d + \frac{p\lambda_m}{L}) &> 0 \\ 2\frac{R}{L}(\frac{R^2}{L^2} + p^2\omega^2) + \frac{R}{L}\frac{p\lambda_m}{L}\frac{p\lambda_m}{J} &> 0 \end{aligned}$$

For positive values of phase resistance R, inductance L, number of rotor teeth p, magnet flux linkage λ_m and inertia J the second criterion for stability will always be satisfied. All of the named parameters will be positive in any stepper motor which means this criterion is actually always satisfied as well. Since $\Delta_4 = e\Delta_3$ the fourth criterion reduces to $e > 0$. This simple fourth criterion is examined first for the sake of simplicity.

$$\begin{aligned} e &> 0 \\ \frac{R}{L}\frac{p\lambda_m}{J}\frac{pV\cos(\delta)}{L} + p\omega\frac{p\lambda_m}{J}\frac{pV\sin(\delta)}{L} &> 0 \\ Rp\lambda_m pV\cos(\delta) + p\omega Lp\lambda_m pV\sin(\delta) &> 0 \\ p\lambda_m pV(R\cos(\delta) + p\omega L\sin(\delta)) &> 0 \\ (R\cos(\delta) + p\omega L\sin(\delta)) &> 0 \\ \sqrt{R^2 + p^2\omega^2L^2}\sin(\delta + \arctan(\frac{R}{p\omega l})) &> 0 \\ \sin\left(\arcsin\left(\frac{p\lambda_m\omega R}{V\sqrt{R^2 + p^2\omega^2L^2}}\right) + \arctan(\frac{p\omega L}{R}) + \arctan(\frac{R}{p\omega l})\right) &> 0 \end{aligned}$$

$$\begin{aligned}
\sin\left(\arcsin\left(\frac{p\lambda_m\omega R}{V\sqrt{R^2+p^2\omega^2L^2}}\right)+\frac{\pi}{2}\right) &> 0\\
0 < \arcsin\left(\frac{p\lambda_m\omega R}{V\sqrt{R^2+p^2\omega^2L^2}}\right) &< \frac{\pi}{2}\\
0 < \frac{p\lambda_m\omega R}{V\sqrt{R^2+p^2\omega^2L^2}} &< 1
\end{aligned}$$

This criterion will always be met when all of the motor parameters are postive, and the voltage is high enough to overcome the emf voltage. This assumption was already made in section 2, so this criterion is always satisfied as well. Because the first, second and fourth stability criteria are always satisfied, stepper motor stability depends only on the third criterion:

$$\begin{aligned}
\Delta_3 &> 0\\
bcd - d^2 - eb^2 &> 0
\end{aligned}$$

in which we have:

$$\begin{aligned}
bcd &= 2\frac{R}{L}\left(\frac{p\lambda_m}{J}(pi_d+\frac{p\lambda_m}{L})+(\frac{R^2}{L^2}+p^2\omega^2)\right)\left(\frac{R}{L}\frac{p\lambda_m}{J}(2pi_d+\frac{p\lambda_m}{L})\right)\\
&= \frac{R^2}{L^2}\frac{p\lambda_m}{J}\left(\frac{p\lambda_m}{J}(2pi_d+2\frac{p\lambda_m}{L})(2pi_d+\frac{p\lambda_m}{L})+2(\frac{R^2}{L^2}+p^2\omega^2)(2pi_d+\frac{p\lambda_m}{L})\right)\\
d^2 &= \left(\frac{R}{L}\frac{p\lambda_m}{J}(2pi_d+\frac{p\lambda_m}{L})\right)^2\\
&= \left(\frac{R^2}{L^2}\frac{p\lambda_m}{J}\right)\frac{p\lambda_m}{J}\left((2pi_d+\frac{p\lambda_m}{L})(2pi_d+\frac{p\lambda_m}{L})\right)\\
eb^2 &= \left(\frac{R}{L}\frac{p\lambda_m}{J}\frac{pV\cos(\delta)}{L}+p\omega\frac{p\lambda_m}{J}\frac{pV\sin(\delta)}{L}\right)\left(2\frac{R}{L}\right)^2\\
&= \frac{R^2}{L^2}\frac{p\lambda_m}{J}\left(4\frac{R}{L}\frac{pV\cos(\delta)}{L}+4p\omega\frac{pV\sin(\delta)}{L}\right)\\
bcd-d^2-eb^2 &= \left(\frac{R^2}{L^2}\frac{p\lambda_m}{J}\right)\left(\frac{p\lambda_m}{L}\frac{p\lambda_m}{J}(2pi_d+\frac{p\lambda_m}{J})+2(\frac{R^2}{L^2}+p^2\omega^2)(2pi_d+\frac{p\lambda_m}{L})\right)\\
&\quad-\left(\frac{R^2}{L^2}\frac{p\lambda_m}{J}\right)\left((4\frac{R}{L}\frac{pV\cos(\delta)}{L}+4p\omega\frac{pV\sin(\delta)}{L})\right)\\
&= \left(\frac{R^2}{L^2}\frac{p\lambda_m}{J}\right)\left((2\frac{R^2}{L^2}+2p^2\omega^2+\frac{p\lambda_m}{L}\frac{p\lambda_m}{J})(2pi_d+\frac{p\lambda_m}{L})-(4\frac{R}{L}\frac{pV\cos(\delta)}{L}+4p\omega\frac{pV\sin(\delta)}{L})\right) \quad (28)
\end{aligned}$$

It is easier to view this stability condition without the term $(\frac{p\lambda_m}{L}\frac{p\lambda_m}{J})$ first. This term will be much smaller then $(2\frac{R^2}{L^2}+2p^2\omega^2)$ for any significantly large value for rotating inertia J. The stability boundary will be shown to lie at exactly $p\omega=\frac{R}{L}$ when this term is neglected. The extra term can be added again later to view its effect. Neglecting this term for now leaves:

$$bcd-d^2-eb^2 = \left(\frac{R^2}{L^2}\frac{p\lambda_m}{J}\right)\left(2(\frac{R^2}{L^2}+p^2\omega^2)(2pi_d+\frac{p\lambda_m}{L})-(4\frac{R}{L}\frac{pV\cos(\delta)}{L}+4p\omega\frac{pV\sin(\delta)}{L})\right)$$

The resulting expression needs to be greater than zero to satisfy the stability criterion:

$$\begin{aligned}
bcd-d^2-eb^2 &> 0\\
\left(\frac{R^2}{L^2}\frac{p\lambda_m}{J}\right)\left(2(\frac{R^2}{L^2}+p^2\omega^2)(2pi_d+\frac{p\lambda_m}{L})-(4\frac{R}{L}\frac{pV\cos(\delta)}{L}+4p\omega\frac{pV\sin(\delta)}{L})\right) &> 0\\
\left(2(\frac{R^2}{L^2}+p^2\omega^2)(2pi_d+\frac{p\lambda_m}{L})-(4\frac{R}{L}\frac{pV\cos(\delta)}{L}+4p\omega\frac{pV\sin(\delta)}{L})\right) &> 0\\
\left((R^2+p^2\omega^2L^2)(pi_d+\frac{p\lambda_m}{2L})-(RpV\cos(\delta)+p\omega LpV\sin(\delta))\right) &> 0
\end{aligned}$$

$$\begin{aligned}
\left((R^2+p^2\omega^2L^2)(i_d+\frac{\lambda_m}{2L})-V(R\cos(\delta)+p\omega L\sin(\delta))\right) &> 0\\
\left((R^2+p^2\omega^2L^2)(i_d+\frac{\lambda_m}{2L})-V\sqrt{R^2+p^2\omega^2L^2}(\sin(\delta+\arctan(\frac{R}{p\omega L})))\right) &> 0\\
\left(\sqrt{R^2+p^2\omega^2L^2}(i_d+\frac{\lambda_m}{2L})-V(\sin(\delta+\arctan(\frac{R}{p\omega L})))\right) &> 0
\end{aligned}$$

The steady state values for i_d and δ from (8a) can be filled in now. They are restated here for sake of clarity:

$$\begin{aligned}
i_d &= \frac{V}{R}\cos\delta\\
\delta &= \arcsin\left(\frac{p\lambda_m R\omega}{V\sqrt{R^2+p^2\omega^2L^2}}\right)+\arctan(\frac{p\omega L}{R})
\end{aligned}$$

When these values are put into the stability condition the following expressions are obtained:

$$\begin{aligned}
\sqrt{R^2+p^2\omega^2L^2}(i_d+\frac{\lambda_m}{2L})-V(\sin(\delta+\arctan(\frac{R}{p\omega L}))) &> 0\\
\sqrt{R^2+p^2\omega^2L^2}(\frac{V}{R}\cos(\delta)+\frac{\lambda_m}{2L})-V(\sin(\delta+\arctan(\frac{R}{p\omega L}))) &> 0\\
\sqrt{R^2+p^2\omega^2L^2}(\frac{V}{R}\cos\left(\arcsin\left(\frac{p\lambda_m R\omega}{V\sqrt{R^2+p^2\omega^2L^2}}\right)+\arctan(\frac{p\omega L}{R})\right)+\frac{\lambda_m}{2L})\ldots&\\
-V(\sin(\arcsin\left(\frac{p\lambda_m R\omega}{V\sqrt{R^2+p^2\omega^2L^2}}\right)+\arctan(\frac{p\omega L}{R})+\arctan(\frac{R}{p\omega L}))) &> 0\\
\sqrt{R^2+p^2\omega^2L^2}(\frac{V}{R}\cos\left(\arcsin\left(\frac{p\lambda_m R\omega}{V\sqrt{R^2+p^2\omega^2L^2}}\right)+\arctan(\frac{p\omega L}{R})\right)+\frac{\lambda_m}{2L})\ldots&\\
-V(\sin(\arcsin\left(\frac{p\lambda_m R\omega}{V\sqrt{R^2+p^2\omega^2L^2}}\right)+\frac{\pi}{2})) &> 0\\
\sqrt{R^2+p^2\omega^2L^2}(\frac{V}{R}\cos\left(\arcsin\left(\frac{p\lambda_m R\omega}{V\sqrt{R^2+p^2\omega^2L^2}}\right)+\arctan(\frac{p\omega L}{R})\right)+\frac{\lambda_m}{2L})\ldots&\\
-V(\cos(\arcsin\left(\frac{p\lambda_m R\omega}{V\sqrt{R^2+p^2\omega^2L^2}}\right)) &> 0
\end{aligned}$$

For $\omega = 0$ the resulting expression evaluates to $\frac{\lambda_m R}{2L}$ which is obviously positive. This means the system is stable for low frequencies. The expression always has negative slope when it is viewed as a function of ω. This means there will be exactly one frequency at which the expression crosses the stability boundary of zero. Above this frequency the stability criterion is not satisfied and the motor is unstable if there is no damping B. It can be shown that this happens at frequency $p\omega = \frac{R}{L}$ by evaluating the expression for exactly this frequency.

$$\begin{aligned}
&\sqrt{R^2+p^2\omega^2L^2}(\frac{V}{R}\cos\left(\arcsin\left(\frac{p\lambda_m R\omega}{V\sqrt{R^2+p^2\omega^2L^2}}\right)+\arctan(\frac{p\omega L}{R})\right)+\frac{\lambda_m}{2L})\ldots\\
&-V(\cos(\arcsin\left(\frac{p\lambda_m R\omega}{V\sqrt{R^2+p^2\omega^2L^2}}\right)))\\
=\ &\sqrt{R^2+\frac{R^2}{L^2}L^2}(\frac{V}{R}\cos\left(\arcsin\left(\frac{\lambda_m R\frac{R}{L}}{V\sqrt{R^2+\frac{R^2}{L^2}L^2}}\right)+\arctan(\frac{\frac{R}{L}L}{R})\right)+\frac{\lambda_m}{2L})\ldots\\
&-V(\cos(\arcsin\left(\frac{\lambda_m R\frac{R}{L}}{V\sqrt{R^2+\frac{R^2}{L^2}L^2}}\right)))\\
=\ &\sqrt{2}R(\frac{V}{R}\cos\left(\arcsin\left(\frac{\lambda_m R}{V\sqrt{2}L}\right)+\arctan 1\right)+\frac{\lambda_m}{2L})-V(\cos(\arcsin\left(\frac{\lambda_m R}{V\sqrt{2}L}\right)))
\end{aligned}$$

$$= \sqrt{2}V\cos\left(\arcsin\left(\frac{\lambda_m R}{V\sqrt{2}L}\right)+\frac{\pi}{4}\right) - V(\cos(\arcsin\left(\frac{\lambda_m R}{V\sqrt{2}L}\right))) + \frac{\lambda_m\sqrt{2}R}{2L}$$

There are some very interesting goniometric equations that can be used here. These are $\cos(\arcsin(x)) = \sqrt{1-x^2}$, and also $\sqrt{2}\cos(\arcsin(x)+\frac{\pi}{4}) = \sqrt{1-x^2}-x$. When these are used the expression reduces to:

$$V\sqrt{1-\left(\frac{\lambda_m R}{V\sqrt{2}L}\right)^2} - V\left(\frac{\lambda_m R}{V\sqrt{2}L}\right) - V\sqrt{1-\left(\frac{\lambda_m R}{V\sqrt{2}L}\right)^2} + \frac{\lambda_m\sqrt{2}R}{2L} = 0$$

This means the condition for stability of (28) shows that the stepper motor is at the edge of instability when $p\omega = \frac{R}{L}$, under the assumption that the damping parameter B equals zero, and that$(\frac{p\lambda_m}{L}\frac{p\lambda_m}{J}) << (2\frac{R^2}{L^2}+2p^2\omega^2)$. When B is greater than zero a lot of extra damping terms are introduced that help the stability, though the frequency at which the motor becomes unstable does change by much.

Also, when the inertia J is very small, $(\frac{p\lambda_m}{L}\frac{p\lambda_m}{J}) << (2\frac{R^2}{L^2}+2p^2\omega^2)$ no longer holds and an extra stabilising term has to be included. This extra term will increase the frequency at which the motor becomes unstable. An insightful description of the stability boundary can be easily deducted from (28), by writing the condition in an orderly fashion:

$$(\sqrt{R^2+p^2\omega^2L^2} + \frac{p\lambda_m L p\lambda_m}{2J\sqrt{R^2+p^2\omega^2L^2}})(i_d+\frac{\lambda_m}{2L}) - V\sin(\delta+\arctan(\frac{R}{p\omega L})) > 0$$

APPENDIX III
STABILITY WHEN DAMPING IS INVOLVED

This appendix aims to do a similar calculation as was made in appendix II but now also including the damping parameter B. Introducing damping into the system increases the stability since the damping will always dissipate energy of any oscillations in the system. The characteristic polynomial of the system is given by $as^4 + bs^3 + cs^2 + ds + e$. The factors in the polynomial are have been calculated in appendix II as 25, and are restated here including the simplification made for d:

$$\begin{aligned} a &= 1 \\ b &= \tfrac{B}{J} + 2\tfrac{R}{L} \\ c &= 2\tfrac{R}{L}\tfrac{B}{J} + \tfrac{p\lambda_m}{J}(pi_d + \tfrac{p\lambda_m}{L}) + (\tfrac{R^2}{L^2} + p^2\omega^2) \\ d &= \tfrac{B}{J}(\tfrac{R^2}{L^2} + p^2\omega^2)) + \tfrac{R}{L}\tfrac{p\lambda_m}{J}(2pi_d + \tfrac{p\lambda_m}{L}) \\ e &= \tfrac{R}{L}\tfrac{p\lambda_m}{J}\tfrac{pV\cos(\delta)}{L} + p\omega\tfrac{p\lambda_m}{J}\tfrac{pV\sin(\delta)}{L} \end{aligned}$$

The system again will be stable when:

$$\begin{aligned} b &> 0 \\ bc - d &> 0 \\ bcd - d^2 - eb^2 &> 0 \\ e &> 0 \end{aligned}$$

It is very easy to show the first, second and fourth stability criteria are still always satisfied. The fourth criterion did not change, and the other two only get positive terms added such that they will still always be satisfied. So again the interesting criterion is the third one:

$$\begin{aligned} bcd - d^2 - eb^2 &= (\tfrac{B}{J} + 2\tfrac{R}{L})(2\tfrac{R}{L}\tfrac{B}{J} + \tfrac{p\lambda_m}{J}(pi_d + \tfrac{p\lambda_m}{L}) + (\tfrac{R^2}{L^2} + p^2\omega^2))(\tfrac{B}{J}(\tfrac{R^2}{L^2} + p^2\omega^2)) + \tfrac{R}{L}\tfrac{p\lambda_m}{J}(2pi_d + \tfrac{p\lambda_m}{L}))\ldots \\ &\quad -(\tfrac{B}{J}(\tfrac{R^2}{L^2} + p^2\omega^2)) + \tfrac{R}{L}\tfrac{p\lambda_m}{J}(2pi_d + \tfrac{p\lambda_m}{L}))^2 - (\tfrac{R}{L}\tfrac{p\lambda_m}{J}\tfrac{pV\cos(\delta)}{L} + p\omega\tfrac{p\lambda_m}{J}\tfrac{pV\sin(\delta)}{L})(\tfrac{B}{J} + 2\tfrac{R}{L})^2 \\ &= \left(\tfrac{B}{J}(\tfrac{R^2}{L^2} + p^2\omega^2) + \tfrac{R}{L}\tfrac{p\lambda_m}{J}(2pi_d + \tfrac{p\lambda_m}{L})\right)\left(2\tfrac{R}{L}((\tfrac{R}{L} + \tfrac{B}{J})^2 + p^2\omega^2) + \tfrac{p\lambda_m}{J}(\tfrac{B}{J}pi_d + \tfrac{B}{J}\tfrac{p\lambda_m}{L} + \tfrac{R}{L}\tfrac{p\lambda_m}{L})\right)\ldots \\ &\quad - (2\tfrac{R}{L} + \tfrac{B}{J})^2\left(\tfrac{R}{L}\tfrac{p\lambda_m}{J}\tfrac{pV\cos(\delta)}{L} + p\omega\tfrac{p\lambda_m}{J}\tfrac{pV\sin(\delta)}{L}\right) \end{aligned}$$

Similar to the nodamping situation, here we have $\frac{p\lambda_m}{J}(\frac{B}{J}pi_d + \frac{B}{J}\frac{p\lambda_m}{L} + \frac{R}{L}\frac{p\lambda_m}{L}) << 2\frac{R}{L}((\frac{R}{L} + \frac{B}{J})^2 + p^2\omega^2)$ for any significant value of rotating inertia J. Assuming enough inertia, that part can be neglected yielding:

$$\begin{aligned} bcd - d^2 - eb^2 &= \left(\tfrac{B}{J}(\tfrac{R^2}{L^2} + p^2\omega^2) + \tfrac{R}{L}\tfrac{p\lambda_m}{J}(2pi_d + \tfrac{p\lambda_m}{L})\right)\left(2\tfrac{R}{L}((\tfrac{R}{L} + \tfrac{B}{J})^2 + p^2\omega^2)\right)\ldots \\ &\quad - (2\tfrac{R}{L} + \tfrac{B}{J})^2\left(\tfrac{R}{L}\tfrac{p\lambda_m}{J}\tfrac{pV\cos(\delta)}{L} + p\omega\tfrac{p\lambda_m}{J}\tfrac{pV\sin(\delta)}{L}\right) \\ &= \left(\tfrac{1}{L^4J}\right)\left(B(R^2 + p^2\omega^2L^2) + Rp\lambda_m(2pi_dL + p\lambda_m)\right)\left(2\tfrac{R}{L}((\tfrac{RJ+BL}{J})^2 + p^2\omega^2L^2)\right)\ldots \\ &\quad - \left(\tfrac{1}{L^4J}\right)\left(\tfrac{2RJ+BL}{J}\right)^2(p\lambda_m pV(R\cos(\delta) + p\omega L\sin(\delta))) \end{aligned}$$

Comparing to the situation without damping the key addition is the term of $B(R^2 + p^2\omega^2L^2)$. This terms is represents the stabilising effect of the damping which obviously increases with frequency. The stability criterion for the motor with significant inertia, and some damping now becomes:

$$\begin{aligned} &\left(B(R^2 + p^2\omega^2L^2) + Rp\lambda_m(2pi_dL + p\lambda_m)\right)\left(2\tfrac{R}{L}((\tfrac{RJ+BL}{J})^2 + p^2\omega^2L^2)\right)\ldots \\ &\quad - \left(\tfrac{2RJ+BL}{J}\right)^2(p\lambda_m pV(R\cos(\delta) + p\omega L\sin(\delta))) > 0 \end{aligned} \tag{29}$$

APPENDIX IV
PROOF OF EQUIVALENCE OF IRTF BASED MODEL AND BASIC MODEL

In this appendix the IRTF based model is inspected more closely. Full mathematical equivalence is proven for the basic stepper motor model given by (1) and the IRTF model introduced in section 1. The electrical part of the IRTF model is shown in vector format in figure 20. All components are complex, with the real part corresponding to phase α and the complex part representing β.

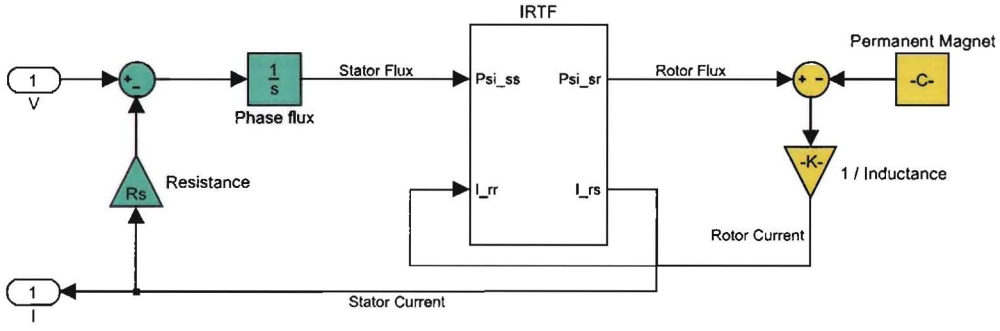

Fig. 20. Electrical part of the IRTF model. Note that this is the vector version of the model such that all the data lines/blocks are two dimensional (complex). The real part always corresponds to phase α, while the imaginary part corresponds to phase β.

To prove equivalence it is shown that the phase currents in the IRTF model obey the same differential equation as in the basic model, and that the torque that is produced by the IRTF is also exactly the same as in the basic model. The notation in the following derivation is superscript 's' for stator current or flux, and superscript 'r' for current/flux in rotor coordinates. The expression for stator current is as follows:

$$\begin{aligned}
I^s &= I^r e^{jp\theta} \\
&= (\Phi^r - \lambda)\frac{1}{L}e^{jp\theta} \\
&= (\Phi^s e^{-jp\theta} - \lambda)\frac{1}{L}e^{jp\theta} \\
&= ((V - I^s R)\frac{1}{s}e^{-jp\theta} - \lambda)\frac{1}{L}e^{jp\theta} \\
sLI^s &= ((V - I^s R)e^{-jp\theta} - s\lambda)e^{jp\theta} \\
&= V - I^s R - s\lambda e^{jp\theta} \\
V &= I^s R + sLI^s + s\lambda ejp\theta \\
&= I^s R + L\frac{dI^s}{dt} + \lambda\frac{d}{dt}e^{jp\theta}
\end{aligned} \tag{30}$$

In (30) the real part corresponds to phase α, and the imaginary part corresponds to phase β. If the real part and the complex part are examined seperately the differential equations for the phases are obtained.

$$\begin{aligned}
v_\alpha &= \Re(V) = \Re\left(I^s R + L\frac{dI^s}{dt} + \lambda\frac{d}{dt}e^{jp\theta}\right) \\
&= i_\alpha R + L\frac{di_\alpha}{dt} + \lambda\frac{d}{dt}\cos(p\theta)
\end{aligned} \tag{31}$$

$$\begin{aligned}
v_\beta &= \Im(V) = \Im\left(I^s R + L\frac{dI^s}{dt} + \lambda\frac{d}{dt}e^{jp\theta}\right) \\
&= i_\beta R + L\frac{di_\beta}{dt} + \lambda\frac{d}{dt}\sin(p\theta)
\end{aligned} \tag{32}$$

The differential equations resulting from the IRTF model that are given by (31) and (32) exactly match the differential equations given in (1a) and (1b). This means the electrical part of the IRTF model behaves exactly according to the basic model of (1). The last equation that needs to be verified is the one for torque. The IRTF produces torque when the flux vector in the motor is not aligned with the current vector. The equation of torque produced by the IRTF is given by:

$$T = -I^s \times \Phi^s$$

Where $\times$ denotes the cross product. The current and flux which are two dimensional vectors are viewed as being three dimensional with the third dimension value being zero. So $I^s = (I_\alpha, I_\beta, 0)$. The resulting torque is then described by:

$$\begin{aligned}
T &= -I^s \times \Phi^s \\
&= -I^s \times (\Phi^r e^{jp\theta}) \\
&= -I^s \times (I^r L + \lambda_m) e^{jp\theta} \\
&= -I^s \times (I^s e^{-jp\theta} L + \lambda_m) e^{jp\theta} \\
&= -I^s \times (I^s L + \lambda_m e^{jp\theta}) \\
&= (-I_\alpha, -I_\beta, 0) \times [(I_\alpha L, I_\beta L, 0) + (\lambda_m \cos(p\theta), \lambda_m \sin(p\theta), 0)] \\
&= (-I_\alpha, -I_\beta, 0) \times (I_\alpha L + \lambda_m \cos(p\theta), I_\beta L + \lambda_m \sin(p\theta), 0) \\
&= (0, 0, -I_\alpha I_\beta L - I_\alpha \lambda_m \sin(p\theta) + I_\beta I_\alpha L + I_\beta \lambda_m \cos(p\theta)) \\
&= (0, 0, -I_\alpha \lambda_m \sin(p\theta) + I_\beta \lambda_m \cos(p\theta))
\end{aligned}$$

Which is again exactly equal to the torque of the basic model described in (1c). Since the describing equations of the basic model (1) are all perfectly matched by the IRTF model, both models are equivalent.